sid.inpe.br/mtc-m21c/2020/04.03.11.42-TDI

USING LAND SURFACE MODELS TO EXPLORE AND IMPROVE ESTIMATIONS OF RESILIENCE OF VEGETATION TO DROUGHTS

Hugo Tameirão Seixas

Master's Dissertation of the Graduate Course in Remote Sensing, guided by Drs. Elisabete Caria Moraes, and Nathaniel Alan Brunsell, approved in March 31, 2020.

URL of the original document:
<http://urlib.net/8JMKD3MGP3W34R/4297UL2>

INPE
São José dos Campos
2020

PUBLISHED BY:

Instituto Nacional de Pesquisas Espaciais - INPE
Gabinete do Diretor (GBDIR)
Serviço de Informação e Documentação (SESID)
CEP 12.227-010
São José dos Campos - SP - Brasil
Tel.:(012) 3208-6923/7348
E-mail: pubtc@inpe.br

sid.inpe.br/mtc-m21c/2020/04.03.11.42-TDI

USING LAND SURFACE MODELS TO EXPLORE AND IMPROVE ESTIMATIONS OF RESILIENCE OF VEGETATION TO DROUGHTS

Hugo Tameirão Seixas

Master's Dissertation of the Graduate Course in Remote Sensing, guided by Drs. Elisabete Caria Moraes, and Nathaniel Alan Brunsell, approved in March 31, 2020.

URL of the original document:
<http://urlib.net/8JMKD3MGP3W34R/4297UL2>

INPE
São José dos Campos
2020

Cataloging in Publication Data

Seixas, Hugo Tameirão.

Se45u Using land surface models to explore and improve estimations of resilience of vegetation to droughts / Hugo Tameirão Seixas. – São José dos Campos : INPE, 2020.

xvi + 70 p. ; (sid.inpe.br/mtc-m21c/2020/04.03.11.42-TDI)

Dissertation (Master in Remote Sensing) – Instituto Nacional de Pesquisas Espaciais, São José dos Campos, 2020.

Guiding : Drs. Elisabete Caria Moraes, and Nathaniel Alan Brunsell.

1. Resilience. 2. Drought. 3. Primary productivity. 4. Land surface model. 5. Caatinga. I.Title.

CDU 528.8:632.112

MINISTÉRIO DA CIÊNCIA, TECNOLOGIA E INOVAÇÕES
INSTITUTO NACIONAL DE PESQUISAS ESPACIAIS

FOLHA DE APROVAÇÃO

A FOLHA DE APROVAÇÃO SERÁ INCLUIDA APÓS RESTABELECIMENTO DAS ATIVIDADES PRESENCIAIS.

Por conta da Pandemia do COVID-19, as defesas de Teses e Dissertações são realizadas por vídeo conferência, o que vem acarretando um atraso no recebimento nas folhas de aprovação.

Este trabalho foi aprovado pela Banca e possui as declarações dos orientadores (confirmando as inclusões sugeridas pela Banca) e da Biblioteca (confirmando as correções de normalização).

Assim que a Biblioteca receber a Folha de aprovação assinada, esta folha será substituída.

Qualquer dúvida, entrar em contato pelo email: pubtc@inpe.br.

Divisão de Biblioteca (DIBIB).

ACKNOWLEDGEMENTS

This study was financed by the National Council for Scientific and Technological Development (CNPq), for granting scholarship.

ABSTRACT

The concept of resilience can be helpful in describing the relationship between vegetation and climate, specially in a context of climate change. However, the quantification and characterization of resilience is a great challenge, due to the high complexity of this concept, and also the difficulty in comparing different ecosystems across the globe. Many studies were already made with the effort of creating methods which enables the comparison between different systems, however, there are still limitations, and there is still space to improve these methods. In order to explore the quantification of resilience of vegetation to drought, we performed a series of simulations by a land surface model (LSM) by manipulating climate data, which was used to estimate the resilience and its components over a dataset with high variation of precipitation regimes. These simulation were performed in the semi-arid region of Caatinga. We also performed an assessment of the LSM performance over the area, in order to give support to the resilience characterization by the model. Results shows that the model was able to represent annual fluxes of water, energy and carbon, and thus, it was possible to use its outputs to estimate the resilience. We also showed that the quantification of resilience can be represented as a function between precipitation variation with gross primary productivity (GPP), which enables a more detailed characterization of the resilience of the vegetation to droughts.

Palavras-chave: Resilience. Drought. Primary productivity. Land surface model. Caatinga.

USANDO MODELOS DE SUPERFÍCIE TERRESTRE PARA EXPLORAR E MELHORAR ESTIMATIVAS DE RESILIÊNCIA DA VEGETAÇÃO A SECAS

RESUMO

O conceito de resiliência pode ser útil para descrever a relação entre vegetação e clima, especialmente em um contexto de mudanças climáticas. No entanto, a quantificação e caracterização da resiliência é um grande desafio, devido à alta complexidade desse conceito e também à dificuldade em comparar diferentes ecossistemas ao redor do mundo. Muitos estudos já foram feitos com o objetivo de criar métodos que possibilitem a comparação entre diferentes ecosistemas, no entanto, ainda existem limitações e ainda há espaço para aprimoramento desses métodos. Para explorar a quantificação da resiliência da vegetação à seca, realizamos uma série de simulações por um modelo de superfície terrestre (LSM), manipulando dados climáticos, que foram utilizados para estimar a resiliência e seus componentes, em um conjunto de dados com alta variação de regimes de precipitação. Essas simulações foram realizadas na região do semi-árido brazileiro (Caatinga). Também realizamos uma avaliação do desempenho do LSM na área, a fim de dar suporte à caracterização da resiliência pelo modelo. Os resultados mostram que o modelo foi capaz de representar fluxos anuais de água, energia e carbono e, portanto, foi possível usar seus resultados para estimar a resiliência da vegetação da área de estudo. Também mostramos que a quantificação da resiliência pode ser representada como uma função entre a variação da precipitação com produtividade primária bruta (GPP), que permite uma caracterização mais detalhada da resiliência da vegetação às secas.

Palavras-chave: Resiliência. Secas. Produção primária. Modelo de superfície terrestre. Caatinga.

LIST OF FIGURES

Page

LIST OF TABLES

Page

CONTENTS

Page

1 INTRODUCTION

Semi-arid regions are highly vulnerable to changes in the vegetation productivity caused by drought events (DU et al., 2018; BENTO et al., 2018; ZSCHEISCHLER et al., 2014b), and although projected changes in drought characteristics with climate change are still uncertain (SIPPEL et al., 2018), the variability of precipitation is likely to increase in a warmer future (PENDERGRASS et al., 2017). In the last decade, the Brazilian semi-arid region faced an extreme drought event considered the most severe in recent decades (MARENGO et al., 2017), with several consecutive years with below average annual precipitations. Dry periods like this can have a significant impact in the vegetation condition, but the relationship between precipitation and vegetation productivity is not yet fully understood (KNAPP et al., 2016). There is also a lack of studies in this subject within the tropics, requiring more regional investigations to allow a better understanding of global impacts of climate extremes on carbon and climate relationship (FRANK et al., 2015).

One possibility to characterize the relationship between vegetation productivity and precipitation regime is to apply the concepts of vegetation resilience to climatic disturbances (LLORET et al., 2011; GAZOL et al., 2016). However, there is still not a consensus over the definition and measurement of resilience, which makes the comparisons across studies and even different ecosystems and variables a challenge (INGRISCH; BAHN, 2018). Resilience can be interpreted more specifically as the capacity of a system to recover from a disturbance, or in a broader sense as an intrinsic ability to maintain its functions before, during and after disturbance events (LAKE, 2012).

Most studies addressing these concepts are based on analysis of field measurements (LLORET et al., 2011; MACGILLIVRAY; GRIME, 1995; STUART-HAëNTJENS et al., 2018; HOOVER et al., 2014; PRETZSCH et al., 2012; GAZOL et al., 2016), which are usually spatially limited, are dependent upon the occurrence of natural disturbance events, and lack the possibility of several measurements along the disturbance and recovery periods. There are many open questions concerning the quantification of resilience, Ingrisch and Bahn (2018) pointed out the importance of investigating how disturbances of different types and severity can affect resilience, what ecosystems are more vulnerable to which kind of disturbance events and what are the resilience of different functions of ecosystems and how they can be compared.

A possible tool to overcome the limitations of reilience quantification could be the use of land surface models (LSM), which enables the possibility of making simulations

across a wide range of spatio-temporal scales of land-atmosphere interactions. This will allow an in-depth characterization of the combined role of vegetation parameters and climatic variability in the vegetation resilience.

1.1 Objectives

This study aims to investigate the response of vegetation resilience to different precipitation regimes, and explore a methodology to compare the resilience of different vegetation types present in the area of study.

To achieve these goals, a series of 49 scenarios composed by a dry (disturbance) and a wet period (recovery), with different intensities and duration for each scenario will be simulated by the Noah-Multiparameterization (NOAH-MP) LSM (NIU et al., 2011). From the model outputs of gross primary productivity (GPP), an index of resilience components will be calculated for GPP and precipitation, following the framework proposed by Ingrisch and Bahn (2018). The resilience will be consist of resistance and recovery components, and this work will explore the relationship of the components calculated for GPP and precipitation to characterize and differentiate the vegetation types.

The study is divided into two chapters, the first is a validation of NOAH-MP performance to estimate carbon and energy fluxes in the region during a period of drought. The validation is performed by comparing the model estimates with field measurements at different time scales, which serves as a foundation to achieve the goals described above. The second chapter addresses the multiple simulations and the resilience analysis of the different vegetation types found in the area of study.

1.2 Questions and hypothesis

To investigate the effects that precipitation variability has on the vegetation, this research has the following hypotheses:

(H1) Land surface models were not specifically developed to estimate resilience of vegetation to droughts, however, since it is able to simulate water, energy, and carbon flux, it is expected that it will be able to represent the resilience phenomenon.

(H2) Stuart-Haëntjens et al. (2018) suggest that the resilience components (impact and recovery) are primarily affected by the mean annual precipitation, and on the concept that a system is the combination of climatic (precipitation) and surface (vegetation productivity) factors. Therefore, it is hypothesised that in order to

characterize the resilience of a given system, it is necessary to analyse the full range of climatic and surface conditions. Since droughts are considered rare events with low coverage, the use of land surface models to create various scenarios of climatic conditions, allows a detailed assessment of resilience of vegetation to droughts.

These hypotheses lead to the following questions:

(Q1) Is NOAH-MP capable of successfully represent water, energy and carbon fluxes in order to generate simulations capable of estimating resilience of vegetation to droughts?

(Q2) How is it possible to use data generated by NOAH-MP to spatialize the quantification of resilience components, and to build a framework capable of comparing the resilience of different vegetation types, by analysing a high amount of precipitation scenarios?

2 LITERATURE REVIEW

2.1 Vegetation resilience

One way to analyze the relationship between precipitation regimes and vegetation state is the use of the concept of vegetation resilience, although its definition and quantification are still divergent across many studies (LAKE, 2012; HODGSON et al., 2015). There are two main conceptions of resilience, the ecological resilience, which considers the capacity of an ecosystem to endure a disturbance effect without changing its state (GUNDERSON, 2000), and the engineering resilience, that approach the stability of a steady state, in which resilience is measurable by the capacity of returning to the equilibrium state (HOLLING, 1996), although different, these two concepts are complementary (INGRISCH; BAHN, 2018).

As a matter of engineering resilience, it also have many different interpretations, and have been developed with time (LAKE, 2012). According to MacGillivray and Grime (1995), the resilience can be defined as the speed of recovery to control levels, in a broader definition, resilience can be characterized as the capacity of a community or individual to recover after a disturbance event to its previous state (LLORET et al., 2011; HOOVER et al., 2014), however, while Lloret et al. (2011) considered resilience to be composed by the concepts of resistance and recovery, in which resistance as the reversal of the impacts caused by the disturbance event, and the recovery as the ability to regenerate relative to the impact of this event, Hoover et al. (2014) used resilience and resistance as two independent measurements. A more detailed description of resilience is given by Hollnagel (2010), in which it is an intrinsic characteristic of a system, and is related to its behavior before, during and after a disturbance event.

The illustration of a system resilience is often described by a period of a disturbance event, followed by a relaxation and a period of recovery that should drive the system to its original state (Figure 2.1) (ZHANG et al., 2010; LLORET et al., 2011; INGRISCH; BAHN, 2018), and within this description, the components that will dictate the quantification of resilience of the system in response to a disturbance also differ among studies. According to Ingrisch and Bahn (2018), resilience can be quantified as a function of measurements of impact (i), which is the change of the system state caused by the disturbance, the perturbation (p), that is the cumulative reduction of the state integrated over the period of recovery, recovery time (r_t) measured by time units from the end of the disturbance period until full recovery, and recovery rate (r_r) that describes the trajectory of the recovery, and can be expressed as the

change of system state per time unit (Figure 2.1).

Figure 2.1 - Schematic illustration of a disturbance and recovery event, showing the different components linked to the concept of resilience.

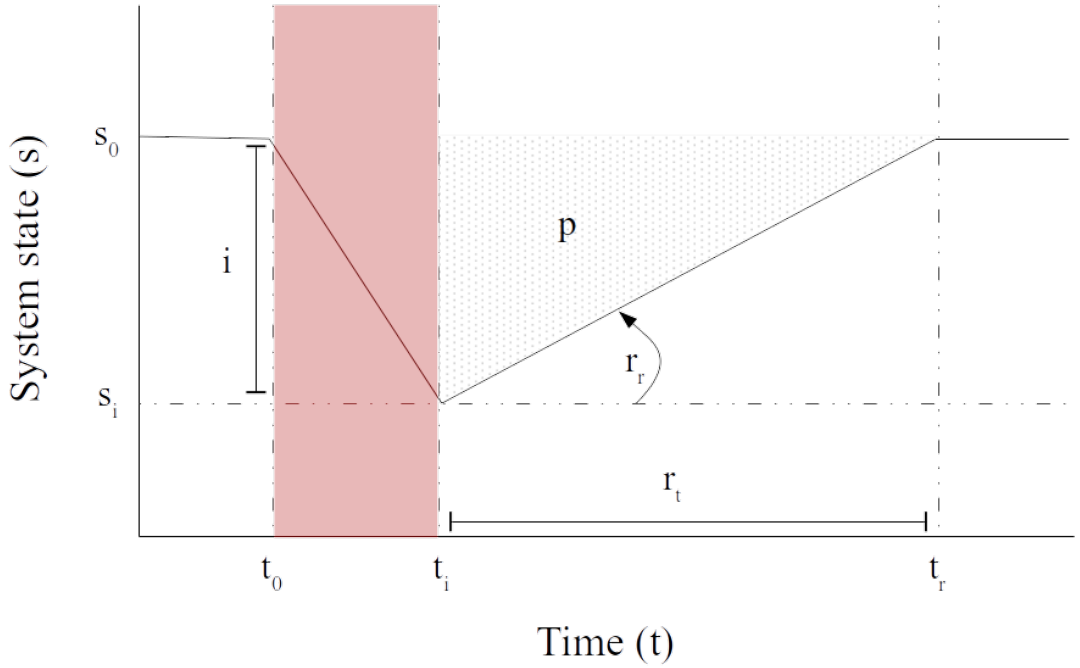

The components are: i (impact), p (perturbation), r_r (recovery rate), r_r (recovery time); t_0 (time before disturbance), t_i (time after disturbance), t_r (time after recovery), s_0 (state before disturbance), s_i (state after disturbance).

SOURCE: Adapted from Ingrisch and Bahn (2018).

Across the studies, it is notable the adoption of components sharing the same name, but with different concepts, the contrary can also happen, as an example, Todman et al. (2016) adopted similar conceptions of some components to describe resilience as Ingrisch and Bahn (2018), but used different nomenclatures, like degree of return, which would be the correspondent of recovery rate, and efficiency for perturbation.

The manner in which these different components are combined can be considered as a metric to quantify resilience, thus can also change how this concept will relate to the disturbance. The quantification of resilience have been made by a wide variety of metrics, according to Ingrisch and Bahn (2018), there are three major groups of metrics that differ from each other, the first category (C1) describes the impact of

the disturbance in relation to a baseline (the state of the system before disturbance), the second (C2) describes the recovery relative to the baseline, and the third (C3) is relative to the disturbance impact.

The table below describes different methods to quantify resilience, from the considered components (Figure 2.1), to the adopted metrics (Table 2.1).

Table 2.1 - List of different resilient metrics and components, classified as category and recovery components.

Category	Recovery Component	Resilience Equation	Reference
C1	Normalized System State	$\frac{s_{t0}}{s_{tr}}$	(LLORET et al., 2011; GAZOL et al., 2016; STUART-HAëNTJENS et al., 2018)
C2	Baseline-Normalized Recovery	$\frac{s_{tr}}{s_{t0}} - \frac{s_{ti}}{s_{t0}}$	(NIMMO et al., 2015)
C3	Impact-Normalized Recovery	$\left\lvert \frac{s_{ti} - s_{t0}}{s_{tr} - s_{t0}} \right\rvert$	(ISBELL et al., 2015)

SOURCE: Adapted from Ingrisch and Bahn (2018).

Hodgson et al. (2015) argue that the characteristics of the resilience of a system cannot be captured in a single metric, but the use of plural features can be better defined and measured in order to address resilience. Furthermore, they point out that in order to conduct a study over resilience, it is crucial to understand the aspects of the system to be studied, the characteristics of the disturbance, the parameters that will be analyzed and the method of quantification of the resilience features for these parameters.

With respect to the resilience of vegetation production parameters in a climatic disturbance scenario, studies have investigated the resilience of different functions, like the use of tree-ring data (LLORET et al., 2011; PRETZSCH et al., 2012; GAZOL et al., 2016; STUART-HAëNTJENS et al., 2018), productivity (HOOVER et al., 2014; ISBELL et al., 2015; STUART-HAëNTJENS et al., 2018), rain-use efficiency (RUE) (DU et al., 2018) and relative water content (RWC) (LI et al., 2012). More specifically in the relation between precipitation regime and vegetation resilience, Stuart-Haëntjens et

al. (2018) found that the resistance and resilience of grasslands and forests were strongly affected by mean annual precipitation rates, and that while the measured resistance were similar for the two types of vegetation, the resilience had divergent responses from each, being that grasslands showed to be more vulnerable than forests. Gazol et al. (2016) observed that the three components of resilience (LLORET et al., 2011) were interrelated, and that resistance and recovery showed a negative relation, which supports that there is a trade-off between these concepts, and that both of them were positively and non-linearly related to resilience. The use of remote sensing data have already been used to quantify resilience components, Keersmaecker et al. (2015) used normalized difference vegetation index (NDVI) measurements in a global scale in a period of 25 years, and found that semi-arid regions showed low recovery and high resistance to drought, although results were not homogeneous between and inside semi-arid regions.

2.2 Relationship precipitation-productivity

The way that vegetation production parameters and precipitation regime relates have an impact over ecological perspectives (KNAPP et al., 2016) (e.g. resilience), however, the relationship between precipitation and primary production is not yet fully understood, showing linear or non-linear relationships (KNAPP et al., 2016). Studies shows that the relationship between these two variables is likely to be non-linear and have positive asymmetric behavior, presenting more sensitivity of above ground net primary production (ANPP) to increased precipitation than to reduced precipitation (KNAPP, 2001; BAI et al., 2008; YANG et al., 2008; WU et al., 2011). On the other hand, there are other studies, conducted using remote sensing estimates and modeling experiments (ZSCHEISCHLER et al., 2014a; LUO et al., 2008; WU et al., 2018), or field experiments where extreme dry and wet conditions were artificially induced over the vegetation (HOOVER et al., 2014; WILCOX et al., 2015), that found evidence that a negative asymmetric relationship can also occur.

The effects of precipitation over the vegetation can still occur after extremes events (e.g. droughts), and also can span from one to more than four years depending on the type of vegetation (SIPPEL et al., 2018). Depending on the climatic conditions after a period of drought, the effects can be amplified or minimized (SIPPEL et al., 2018).

3 ASSESSING THE CARBON, ENERGY AND WATER RESPONSES TO AN EXTREME DROUGHT IN BRAZILIAN CAATINGA USING EDDY COVARIANCE AND NOAH-MP

3.1 Introduction

Recent studies point to an increase in droughts events in the twenty-first century in different regions of the planet, mainly caused by changes in precipitation variability and intensity, increase of evaporative demand, and rising temperature (DAI et al., 2018; DAI; ZHAO, 2016; ZHAO; DAI, 2016). While there are large uncertainties in quantifying drought trends, including the limitations of drought indices and issues with forcing data sets (SHERWOOD; FU, 2014; TRENBERTH et al., 2013; DAI; ZHAO, 2016; ZHAO; DAI, 2016), it is expected that droughts are going to be a major challenge in a warmer climate. In the last two decades many extreme drought events have occurred in Brazil (ORLOWSKY; SENEVIRATNE, 2013; SPINONI et al., 2015), such as in 2005, 2010 and 2015/2016 in the Amazon (MARENGO et al., 2008; LEWIS et al., 2011; ANDERSON et al., 2018) and in 2011/2012 in the Cattinga (MARENGO et al., 2017).

The semi-arid region of Brazil suffered an extreme drought event that lasted from 2011/2012 to 2017, being considered the most severe in the last few decades (MARENGO et al., 2017; CUNHA et al., 2019). It is suggested that droughts in this region have become more frequent, severe, and with higher percentage of affected areas (BRITO et al., 2018). Future projections indicate a higher frequency of consecutive dry days, although precipitation projections are highly uncertain as to whether there will be an increase or decrease of precipitation (MARENGO et al., 2017). Although the Caatinga have been poorly studied in comparison to Brazilian tropical forests, it is known that semi-arid regions are important in controlling the inter-annual variability and magnitude of the global carbon cycle (POULTER et al., 2014; AHLSTROM et al., 2015). It is of upmost importance to determine how droughts will impact the water and carbon cycling in this region (HUANG et al., 2016), and to improve Land Surface Models (LSMs) simulations (AHLSTROM et al., 2015).

Using LSMs to represent land-atmosphere interactions in coupled simulations with climatic models is essential for understanding how energy, water and carbon fluxes can be affected by climate and land cover in conjunction with climate change projections (PRENTICE et al., 2015). However, there are limitations in LSM simulations of surface-atmosphere feedbacks (e.g. droughts), such as the inability of distinguishing the differential responses of each plant functional type (PFT) to water availability

(KAUWE et al., 2015). A better representation of these interactions is key to improve future projections of global warming scenarios.

The validation of LSMs with observed measurements is necessary to provide information on how models can be enhanced, by diagnosing where models fail to represent the surface-atmosphere interactions. Recently, a number of models intercomparison projects have been developed, enabling the comparison of outputs from a wide number of LSMs with observed data and benchmarks based on linear and nonlinear regressions (BEST et al., 2015; COLLIER et al., 2018). These projects enable the identification of differences between models over different areas, and have a high potential to support the understanding on how to improve models. However, there are still limitations concerning how to turn the results into clear diagnostics of model performance (NEARING et al., 2018). To understand how a LSM is performing under extreme events (e.g. droughts), it is necessary to make a more detailed assessment between modelled outputs and field measurements. However, this kind of validation is still scarce in the literature (KAUWE et al., 2015). Based on considerations above, we propose to assess the NOAH-MP estimations of carbon, energy and water responses to an extreme drought event from 2011 to 2012 in the Caatinga biome.

3.2 Material and methods

3.2.1 Area of study

The study area is located in the semi-arid region of northeast Brazil, in the western portion of the Pernambuco (PE) state (Figure 3.1).

The flux tower is located in Petrolina (PE)(40°19'18.38"W; 9°2'45.66"S), inside an area of 600 ha (6 km^2) of preserved Caatinga vegetation, which is part of Brazilian Agricultural Research Corporation (Embrapa) Semi-Arid site. The preserved Caatinga area is mostly composed by shrub arboreal hyperxerophilic vegetation, with an average height of 5 meters (SOUZA et al., 2018). Some of the predominant species are *Mimosa tenuiflora*, *Cnidoscolus phyllacanthus*, *Poincianella microphylla*, *Croton conduplicatus*, *Bauhinia cheilantha*, *Manihot pseudoglaziovii*, *Commiphora leptophloeo* (DRUMOND et al., 2002; SOUZA et al., 2018). The vegetation in this area lose their leaves in the dry periods of the year, usually from May to September, producing new leaves from October to April.

Figure 3.1 - Location of the study area in the Brazilian territory, and the flux tower and meteorological station, accompanied by the total annual precipitation time series.

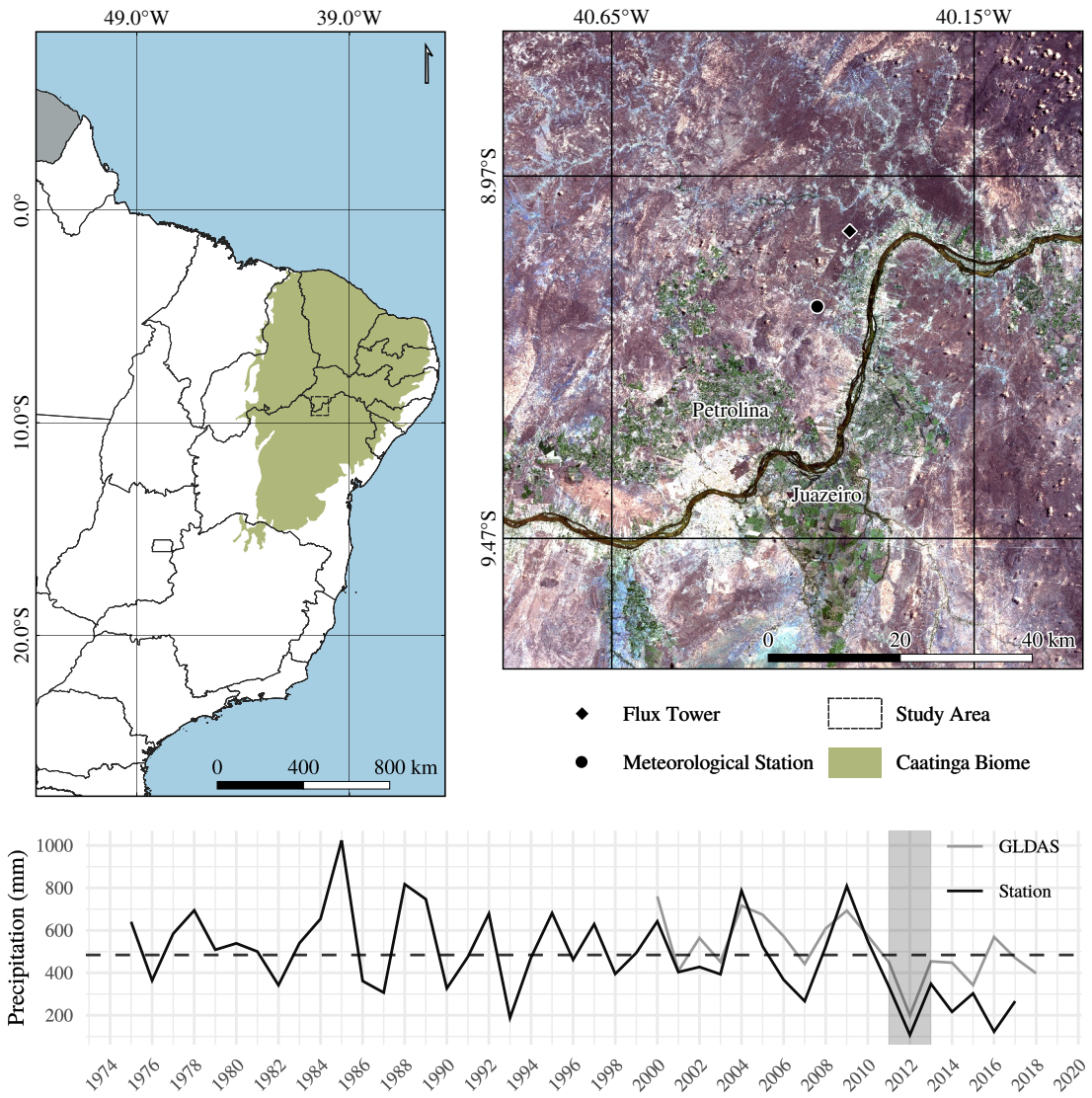

The gray shaded area represents the period that the present study, the black line is the historical annual precipitation measured by the station, the gray line is the annual precipitation estimated by the Global Land Data Assimilation System (GLDAS). The satellite image is a true color composite, derived from Sentinel 2 collection from 21/09/2019.

SOURCE: Own production.

Monthly meteorological data ranging from 1975 to 2018, shows that the study area has a mean annual precipitation of 490 mm with the driest year having 107 mm (2012) and the wettest having 1023 mm (1985) (Figure 3.1). The rainfall usually

occurs from November to May, although its distribution is highly variable throughout the year. Most of total annual precipitation can be concentrated in one or two months in some years, or show precipitation distributed between November to May in other years. In dry years, a majority of the rainfall tends to concentrate in January, February or March.

The last extreme drought event recorded in this region started in the end of 2011 due to abnormal conditions during a La Niña event, in addition with a negative Atlantic Dipole in the beginning of 2012. This was the period of most severe drought conditions from 2011 to 2017. A strong El Niño event that occurred between 2015/2016 extended even further this dry period duration (CUNHA et al., 2019).

3.2.2 Datasets

3.2.2.1 NOAH-MP

The NOAH-MP is an improved version of NOAH-LSM, including multiple options to parameterize the vegetation canopy surface energy balance, frozen soil and snow, groundwater interaction with soil, surface runoff and ground water discharge, and vegetation dynamics (NIU et al., 2011).

The model was configured to run with a spatial resolution of 1km. The scale and resolution were defined based on a balance between computational cost, representativeness of the region, and the ability to distinguish the different land cover types within the study area.

We utilized the NASA Global Land Data Assimilation System (GLDAS) data for meteorological forcing, with a spatial resolution of 0.25 degrees every three hours (RODELL et al., 2004). The GLDAS forcing data were interpolated to intervals of one hour to run NOAH-MP.

The dynamic vegetation was parameterized using the maximum fractional vegetation, which uses a Ball-Berry type stomatal resistance. We used the NOAH formulation for the soil moisture factor controlling stomatal resistance. The adopted run-off and groundwater scheme were the TOPMODEL with simple groundwater, the surface exchange coefficient for heat was based on Monin-Obukhov similarity theory, and the radiation transfer was represented by a two-stream scheme for the vegetated fraction. More details of the the option schemes are described in Niu et al. (2011).

In order to compare the model outputs with field observations, values of the cell which included the coordinates of the flux tower were extracted using nearest neighbor sampling. The representation of the land cover adopted in the model runs is from the MODIS landcover product MCD12Q1, collection 5 (FRIEDL, 2015). The classification of the landcover in the extracted cell, where the tower flux is located, is open shrublands, according to the MCD12Q1 product following the IGBP classification scheme.

3.2.2.2 Field measurements

The eddy covariance tower collected data for latent heat (LE), net ecosystem exchange (NEE), sensible heat flux (H), global solar radiation (Rs), air temperature (T_a), relative humidity (RH), soil temperature (T_s), vapour pressure deficit (VPD) and CO2 concentration (ρ_C). More information about the measurements and methodology can be found in Souza et al. (2018).

The tower measurements were processed using the REddyProc R package, where environmental and flux measurements gaps were filled, followed by the partitioning of net ecosystem exchange into gross primary productivity (GPP) and ecosystem respiration (R_{eco}) using the methodology proposed by Keenan et al. (2019). Observed outliers in NEE, LE, and H were removed by the application of a z-score threshold of three standard deviations. The evapotranspiration (ET) was also calculated based on LE and T_a within the same package.

3.2.3 Data analysis

To analyse the performance of NOAH-MP to model carbon, energy and water fluxes, a selection of metrics were calculated. The modified coefficient of efficiency (E_1) proposed by Legates and McCabe (1999) was chosen as a dimensionless index to quantify model accuracy, followed by the error measures of mean absolute deviation (MAD), mean absolute error (MAE), mean bias error (MBE), normalized mean error (NME), standard deviation metric (SD) (BEST et al., 2015), and the percent bias (PBIAS).

The modified coefficient of efficiency (E_1) is based in the coefficient of efficiency (E) proposed by Nash and Sutcliffe (1970), a common metric widely used to validate hydrologic models. The E_1 was selected for this study due to its easy interpretation (especially in the positive range), decreased impact of outliers and large deviations, and as a commonly used metric it facilitates comparison across studies. The general

form of the coefficient of efficiency can be computed as:

$$E_j = 1.0 - \frac{\sum_{i=1}^{n} |P_i - O_i|^j}{\sum_{i=1}^{n} |O_i - \overline{O'}|^j} \tag{3.1}$$

where P_i is the predicted value, O_i the observed value, both are paired values in a series of n elements, $\overline{O'}$ is the baseline predictor to be compared with observation values, and j is the scaling coefficient.

Legates and McCabe (1999) suggested a modified version in which $j = 1$ due to the fact that the use of absolute values of the differences does not overemphasize outliers, as the original version proposed by Nash and Sutcliffe (1970). In its general form, the index is calculated using the mean of all observed values as the baseline to access model performance. However, for strongly seasonal series, a static value such as the mean is not a good predictor and can lead to overestimation of model performance (LEGATES; MCCABE, 2013; SCHAEFLI; GUPTA, 2007). A possible solution is to present the result of the performance index using alternative predictors in addition to the mean, since it is an easily interpretable and comparable baseline (WILLMOTT et al., 2015).

In this study, three other predictors were used in addition to the mean. We used an aggregated mean for different time scales, where $\overline{O}^h$ is the hourly mean of each season (dry and rainy), representing hourly fluctuation through the day, $\overline{O}^d$ is the daily mean, which removes the hourly variability but keeps a fine time scale, and $\overline{O}^m$ as the monthly mean, representing a coarser time scale with less variability and closer to the overall mean as predictor. The calculated E_1 at each of these timescales will be referenced as E_1^h, E_1^d, and E_1^m respectively.

The mean error and deviation metrics MAE and MAD are compliments of E_1, since models with poor performance will present $MAE > MAD$. These metrics are useful at describing the relation between model error and the baseline deviation with observations. The MBE describes the difference of the mean between predicted and observed values, and is useful to indicate if the model is over or under predicting the observations. However, these metrics maintain the units of the original data, making it difficult to compare between different variables, which can be achieved using a normalized error metric such as the NME to compare the error between observations and predictions, and PBIAS to compare the bias. These metrics are

expressed as:

$$MAE = \frac{1}{n}\sum_{i=1}^{n}|P_i - O_i| \tag{3.2}$$

$$MAD = \frac{1}{n}\sum_{i=1}^{n}|O_i - \overline{O'}|^j \tag{3.3}$$

$$MBE = \frac{1}{n}\sum_{i=1}^{n}(P_i - O_i) \tag{3.4}$$

$$NME = \frac{\sum_{i=1}^{n}|P_i - O_i|^j}{\sum_{i=1}^{n}|\overline{O'} - O_i|^j} \tag{3.5}$$

$$PBIAS = \frac{\sum_{i=1}^{n}(P_i - O_i)}{\sum_{i=1}^{n}|O_i|} * 100 \tag{3.6}$$

The standard deviation metric proposed by Best et al. (2015) to benchmark different LSMs is useful to explore differences in variability between predicted and observed values:

$$SD = \left| 1 - \frac{\sqrt{\frac{\sum_{i=1}^{n}(P_i - \overline{P})}{n-1}}}{\sqrt{\frac{\sum_{i=1}^{n}(O_i - \overline{O})}{n-1}}} \right| \tag{3.7}$$

All the metrics cited above were calculated over the hourly values of gap filled series of each variable. The use of gap filled data over the original measurements was preferred because of its impact in the aggregation of data to coarser time scales, which would have bigger impacts in the annual balance of carbon fluxes.

In order to investigate the coupled responses between the carbon and water cycles, we calculated the water-use efficiency (WUE):

$$WUE = \frac{GPP}{ET} \tag{3.8}$$

The temporal relationships between precipitation and the carbon and energy fluxes were analysed through the cross-lagged correlation between these variables.

Periods between January to May (2011), October (2011) to February (2012) and November to December (2012) were considered as rainy periods, and the ones between June to September (2011) and March to October (2012) as dry periods.

3.3 Results

The annual balance of carbon, energy fluxes and total precipitation were first analysed to provide an overview of values from both sources (Figure 3.2). In 2011 the total precipitation was overestimated by GLDAS (476 mm), a value close to the historical mean measured by the meteorological station. The station measured 283 mm of precipitation for 2011. The cumulative NEE for 2011 shows that NOAH-MP estimated a larger sink of carbon from the atmosphere (-371 $\mathrm{g\,m^{-2}\,y^{-1}C}$) than the observed values (-174 $\mathrm{g\,m^{-2}\,y^{-1}C}$). However, the GPP and R_{eco} were significantly underestimated by the model in 2011, with a difference of 47.2% and 73.7%, respectively. In 2012, the precipitation was lower for modeled and observed values (195 mm and 141 mm, respectively). When compared to 2011, the NEE showed that the vegetation acted as a source of carbon to the atmosphere. In this case the tower value (186 $\mathrm{g\,m^{-2}\,y^{-1}C}$) was higher than NOAH-MP (79 $\mathrm{g\,m^{-2}\,y^{-1}C}$), as well as for GPP and R_{eco}, which were still underestimated by NOAH-MP as in 2011, but with smaller differences of 41.6% and 54.6% respectively. The LE was overestimated by NOAH-MP in both years, with a significant drop in 2012, while H was underestimated by the model, and had a smaller increase in 2012.

The reduction of precipitation from 2011 to 2012 was 59% according to modeled data from GLDAS. This is a difference of 281mm, while the measurements from the meteorological station show a reduction of 50%, a decrease of 142mm (Figure 3.2). The modeled rainfall points a more severe decrease in 2012, which is reflected in a stronger impact over the absolute values of NEE in NOAH-MP with a difference of 447 $\mathrm{g\,m^{-2}\,y^{-1}C}$ compared to 360 $\mathrm{g\,m^{-2}\,y^{-1}C}$ from the tower. However, these differences represents a change of 120% and 200% respectively, which shows that the model seems to underestimate the impact of the drought over NEE. The GPP reduced 85% for the model and 86% for the tower, and R_{eco} reduced 42% (model) and 66% (tower). This suggests that although the absolute values of GPP show

significant deviations between the model and observations, the proportional response to the drought was similar, while those differences were greater for R_{eco}.

Figure 3.2 - Comparison of annual values from NOAH outputs and field based estimates of carbon, energy and water fluxes.

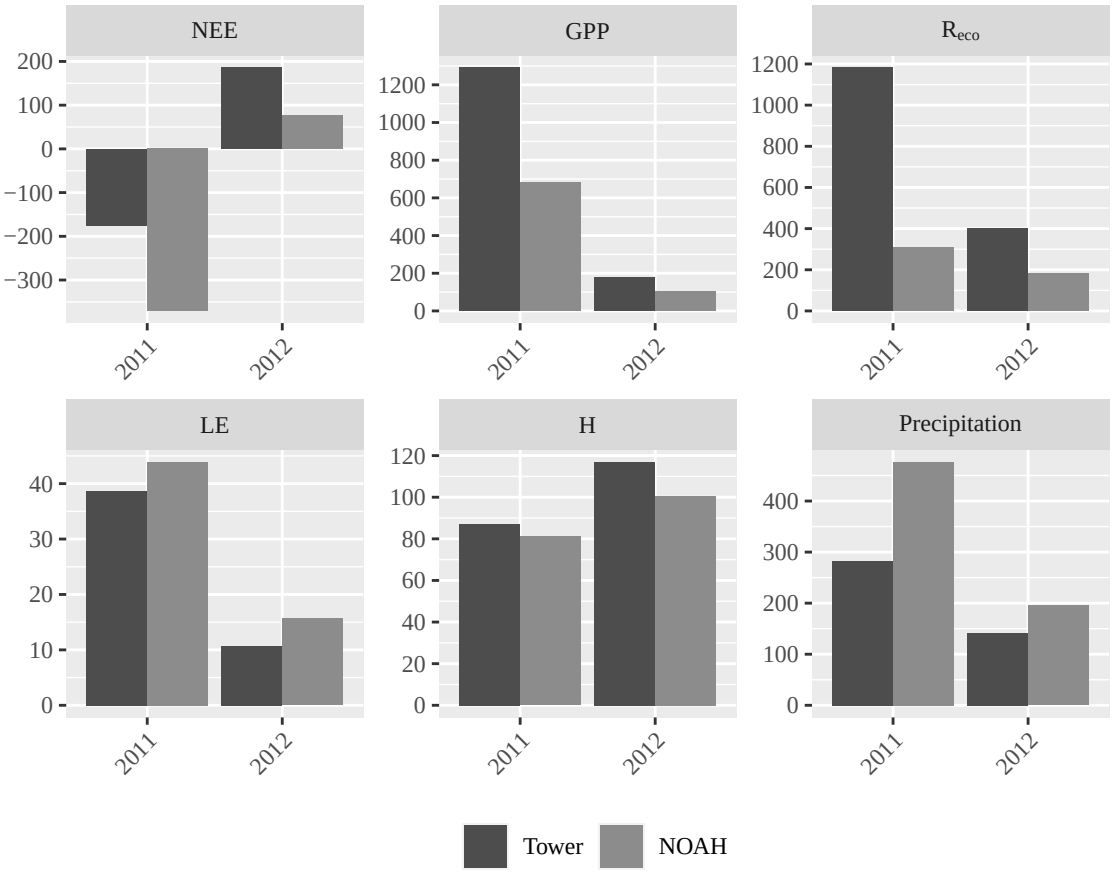

The fluxes are represented as NEE ($\mathrm{g\,m^{-2}\,y^{-1}C}$), GPP ($\mathrm{g\,m^{-2}\,y^{-1}C}$), R_{eco} ($\mathrm{g\,m^{-2}\,y^{-1}C}$), LE ($\mathrm{W\,m^{-2}}$), H ($\mathrm{W\,m^{-2}}$) and total precipitation (mm).

SOURCE: Own production.

Monthly accumulated values were analysed in order to assess the agreement of seasonality within the years between the two sources (Figure 3.3). The scatter plots show that there is a general agreement across the monthly values, with larger divergences pointed by the slope of GPP, R_{eco} and H (0.43, 0.14 and 0.53, respectively). The largest deviations were in R_{eco}, which shows less agreement between modeled values and tower derived values. Even with significant differences in precipitation

for each year (Figure 3.2), the seasonality is well represented across the years, and this is translated to a positive correlation in carbon and energy fluxes.

Figure 3.3 - Scatter plot of monthly values from NOAH-MP outputs and field derived estimates of carbon, energy and water fluxes.

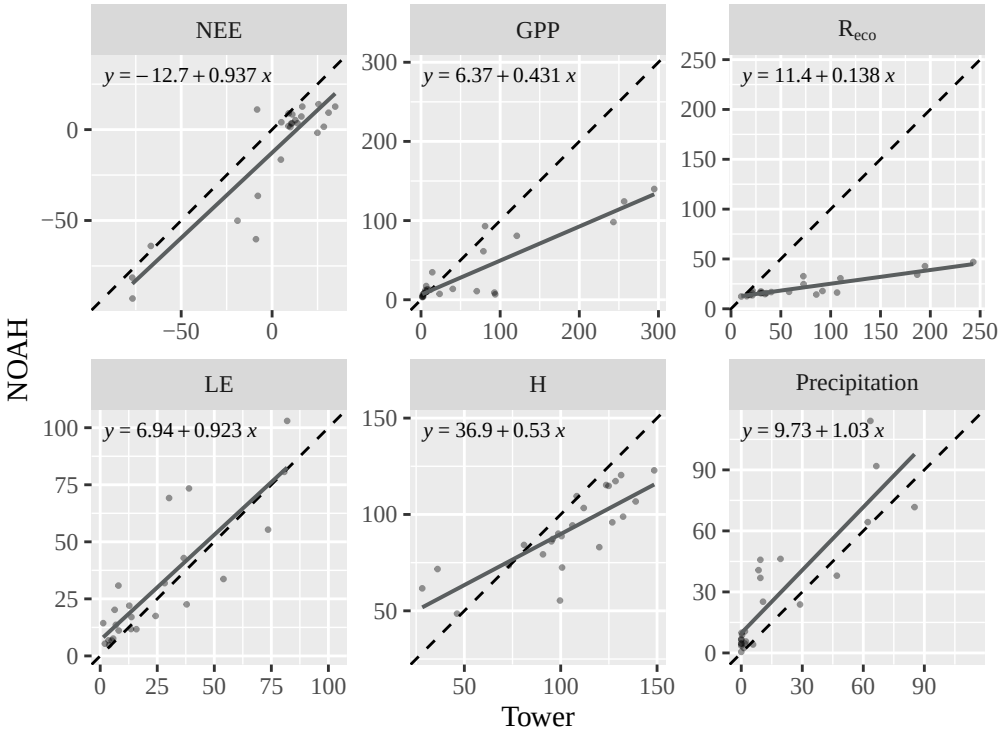

The fluxes are represented as NEE ($\mathrm{g\,m^{-2}\,y^{-1}C}$), GPP ($\mathrm{g\,m^{-2}\,y^{-1}C}$), R_{eco} ($\mathrm{g\,m^{-2}\,y^{-1}C}$), LE ($\mathrm{W\,m^{-2}}$), H ($\mathrm{W\,m^{-2}}$) and total precipitation (mm).

SOURCE: Own production.

When values are analysed at a daily scale (Figure 3.4), it is possible to see a lack of agreement between the NOAH-MP estimates and the tower data for the carbon fluxes and precipitation. The energy fluxes exhibit relationships similar to those found at the monthly scale (Figure 3.3), with the expected larger variance. The precipitation values indicate that even having good agreement in monthly seasonality, the daily values of rainfall are not in agreement, where the GLDAS exhibits more days with low amounts of rainfall, while the field measurements show more days without rainfall, where the precipitation is concentrated in fewer days.

Figure 3.4 - Scatter plot of daily values from NOAH-MP outputs and field derived estimates of carbon, energy and water fluxes.

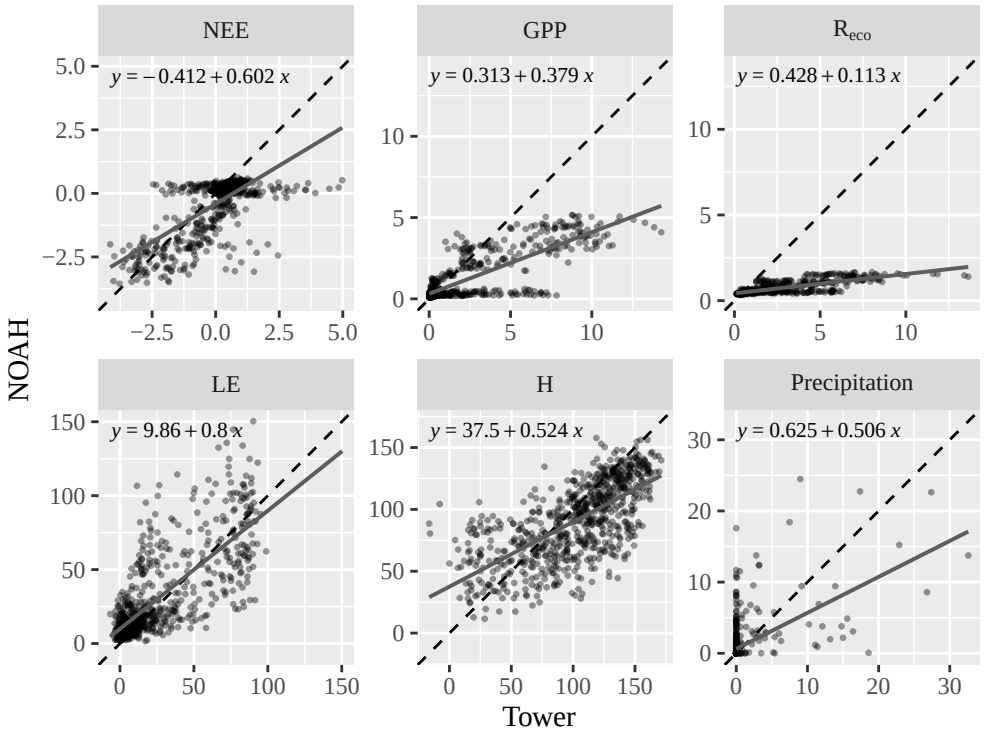

The fluxes are represented as NEE ($\mathrm{g\,m^{-2}\,y^{-1}C}$), GPP ($\mathrm{g\,m^{-2}\,y^{-1}C}$), R_{eco} ($\mathrm{g\,m^{-2}\,y^{-1}C}$), LE ($\mathrm{W\,m^{-2}}$), H ($\mathrm{W\,m^{-2}}$) and daily precipitation (mm).

SOURCE: Own production.

Similar to the monthly data, the daily time series of precipitation confirms that the GLDAS was able to capture the seasonality of precipitation (Figure 3.5), although there are more rainfall events during the dry periods.

From the daily time series, the modeled NEE shows less variability than the observed data. The tower data exhibits abrupt pulses of NEE after rainfall events, while NOAH-MP does not exhibit such behavior (Figure 3.5). There was an overall overestimation by NOAH-MP of negative NEE during the first rainfall period (January to May, 2011) taking longer to start showing net respiration at the daily scale ($R_{eco} > 0$) during the subsequent dry period. The observed data shows a predominance of net respiration at the daily scale from the beginning of July through October. NOAH-MP showed little sensitivity to rainfall during the second wet period (October, 2011 to February, 2012), with the predominance of positive daily NEE.

These values started to decrease after the end of February, while the observed values showed large negative peaks following rainfall events.

Figure 3.5 - Daily time series of daily carbon, energy and water fluxes.

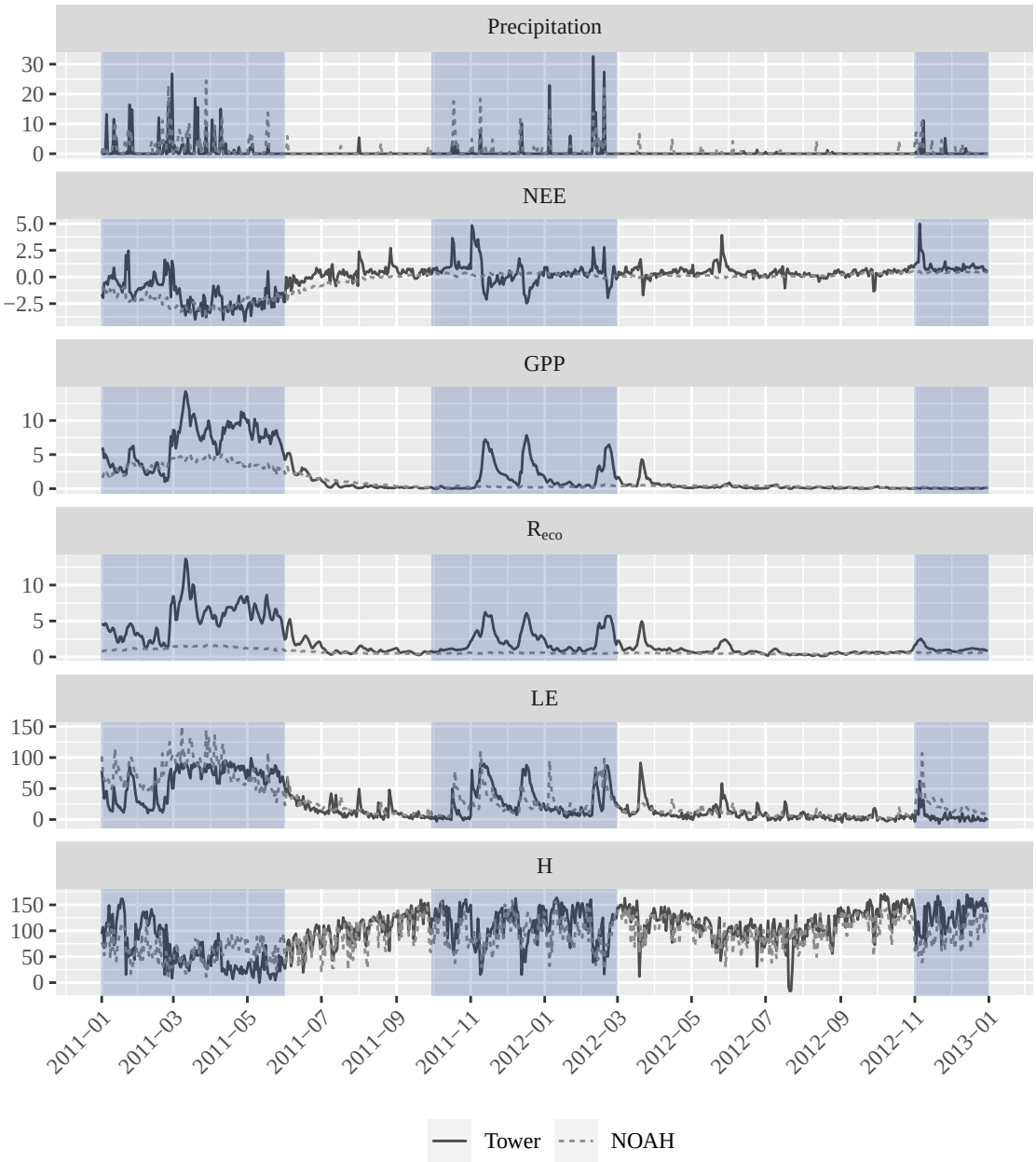

The fluxes are represented as daily precipitation (mm), NEE ($\mathrm{g\,m^{-2}\,y^{-1}C}$), GPP ($\mathrm{g\,m^{-2}\,y^{-1}C}$), R_{eco} ($\mathrm{g\,m^{-2}\,y^{-1}C}$), LE ($\mathrm{W\,m^{-2}}$) and H ($\mathrm{W\,m^{-2}}$). Blue shaded areas indicates the rainy periods.

SOURCE: Own production.

The model underestimated GPP in 2011 from January to May, although its values have a slower decrease in the subsequently dry months when compared to the observed data. The precipitation increased again around October, when even lower amounts of rain lead to rapid increases in the observed GPP, followed by a rapid decrease. This behavior is not observed in the modelled output, where the GPP only exhibited a slight increase at the end of March (2012). This increased GPP persisted through the dry months (April to October in 2012).

The R_{eco} was also underestimated by NOAH-MP, showing little variation through the years, with a perceptive increase only in the first rainy season (January to May, 2011). The observed data showed peaks of ecosystem respiration after rainfall events with rapidly decreasing values after days without rain (Figure 3.5).

The increased precipitation in the beginning of 2011 resulted in modeled LE values reaching a higher peak along with heavier rainfall. This was not observed in the field data, where the LE reached an upper limit during wet periods, maintaining relatively constant values through this period only decreasing a few weeks into the dry season (Figure 3.5). The modelled data showed a different behavior, with the diminishing rains at the end of the wet period resulting in a smoother decrease in LE that is maintained until the begin of the next rainy season. Although the observed LE values are lower than the ones obtained by the model, it seems to be more responsive to lower amounts of rain, which can be seen as peaks during the dry period.

The water use efficiency estimated from the model showed lower values during the rainy periods (Figure 3.6), with a small increase during the dry periods. This is caused by the faster decrease of GPP (in relation to ET) after the end of the first wet season. During the second wet period, the WUE dropped substantially due to the increase of ET caused by the increased rain and the lack of GPP response. This behavior contrasts with the tower data, which exhibited large values during the wet periods, caused by the high GPP and the rapid response to precipitation, and lower values during the dry season. It is possible to observe that the decrease of GPP after the end of rainfall events is slower than for ET, resulting in a maintenance of WUE for a period following precipitation events. The general higher WUE from the tower data explains the large differences observed in annual scale 3.2, which shows that even with higher annual precipitation, NOAH-MP still underestimated annual GPP.

Figure 3.6 - Daily WUE for the model output and flux tower estimates, and daily values of ET and GPP.

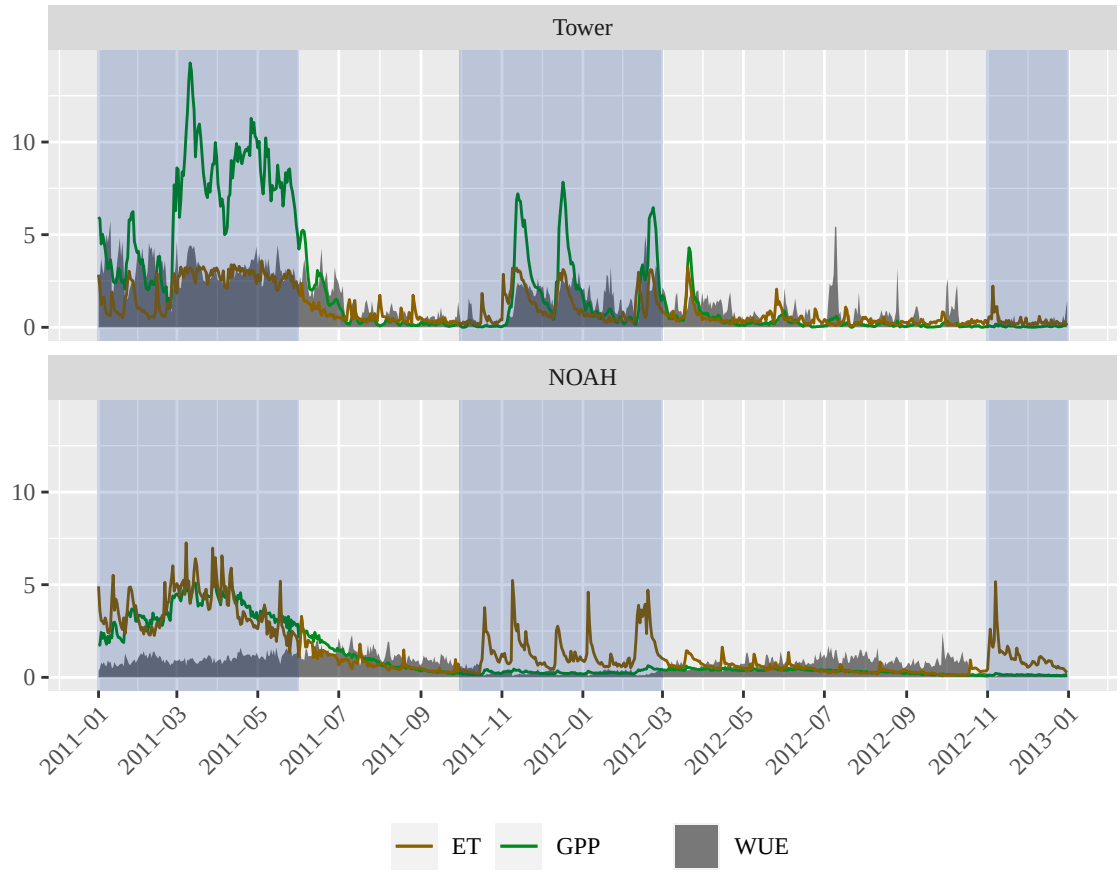

The daily WUE is represented by the gray area, daily values of ET (mm/day) by the brown lines and GPP ($\mathrm{g\,m^{-2}\,y^{-1}C}$) by the green line. Blue shaded areas indicates the rainy periods.

SOURCE: Own production.

In order to assess the different responses to precipitation we utilized the cross correlation between precipitation and the carbon and energy fluxes (Figure 3.7). The modeled carbon fluxes exhibited a higher correlation with time lags after the precipitation events, probably due to the reduced variability in these values (Figure 3.5). The tower data showed a peak in the correlation approximately 10 days after precipitation events. The cross correlation between GPP and ET exhibited a stability of correlation in the model, that is presumably due to the lack of variability in the GPP.

Figure 3.7 - Lag correlation of carbon and energy fluxes against precipitation, and between ET and GPP.

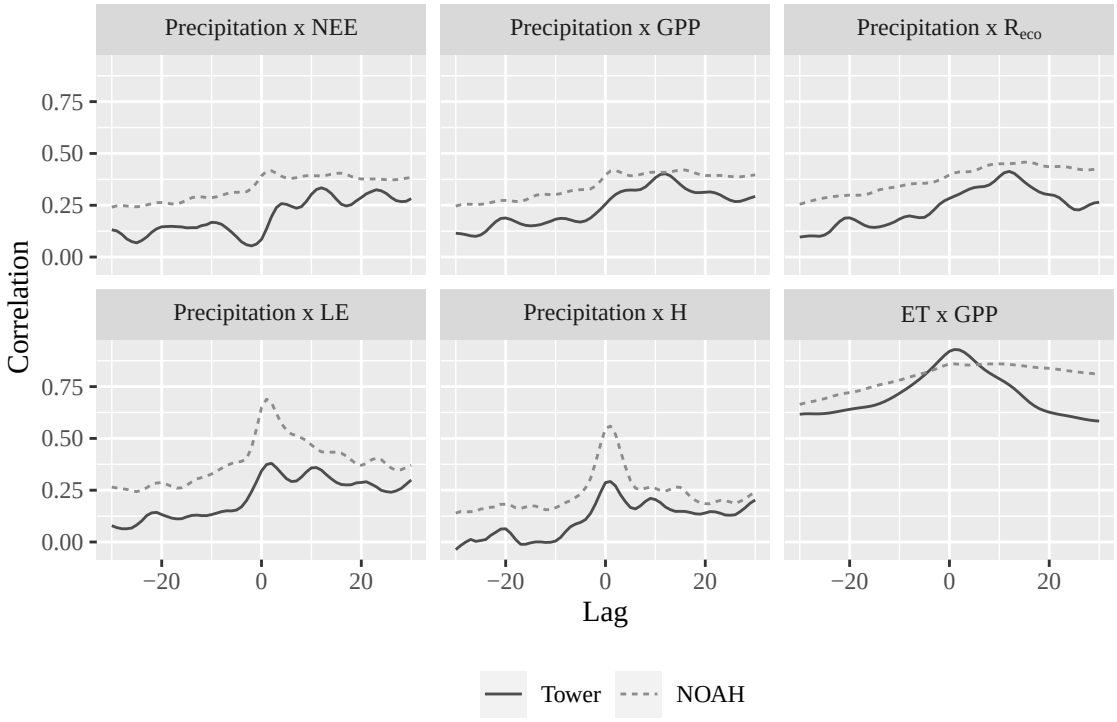

The correlation was calculated over a rolling mean of three days in order to facilitate the interpretation of the graphs. Lags are expressed in number of days. The correlation of NEE and H were multiplied by -1 to facilitate interpretation.

SOURCE: Own production.

The hourly values of carbon and energy fluxes for 2011 and 2012 were analysed in order to have a detailed assessment of NOAH-MP performance. The selected metrics for model comparison show some superficial differences between the two sources (Table 3.1).

It is possible to observe that field measurements of NEE exhibited a larger variance than the modeled data, with peak values that are not observed in the NOAH-MP output. The mean modeled NEE is negative (-0.017 $\mathrm{g\,m^{-2}\,y^{-1}C}$), while the observed values show a positive mean closer to zero (0.001 $\mathrm{g\,m^{-2}\,y^{-1}C}$). As the values become more extreme, we observed larger differences between the modelled and tower data. A similar behaviour is observed for the extreme values (between the 75th and 95th percentiles) of GPP and $Reco$ (which are components of NEE). The observed LE

Table 3.1 - Exploratory statistics of carbon and energy fluxes from NOAH-MP output and field measurements.

Var	Source	Min	5_{th}	25_{th}	Mean	75_{th}	95_{th}	Max	Std
NEE	NOAH	-0.498	-0.221	-0.007	-0.017	0.017	0.027	0.056	0.080
	Tower	-1.105	-0.343	-0.004	0.001	0.054	0.190	1.011	0.166
GPP	NOAH	0.000	0.005	0.016	0.091	0.090	0.396	0.669	0.132
	Tower	0.000	0.000	0.006	0.163	0.188	0.848	1.640	0.277
R_{eco}	NOAH	0.009	0.011	0.014	0.028	0.031	0.087	0.171	0.024
	Tower	0.000	0.012	0.029	0.090	0.119	0.303	0.913	0.102
LE	NOAH	-12.72	0.012	3.64	29.59	30.64	136.4	511.6	49.87
	Tower	-67.95	-11.18	-1.43	24.66	27.19	155.3	252.6	49.81
H	NOAH	-103.6	-26.05	-8.53	90.98	179.4	384.2	546.6	137.0
	Tower	-82.83	-34.58	-17.11	101.9	202.1	470.3	611.8	170.6

The fluxes are represented as NEE ($\mathrm{g\,m^{-2}\,y^{-1}C}$), GPP ($\mathrm{g\,m^{-2}\,y^{-1}C}$), R_{eco} ($\mathrm{g\,m^{-2}\,y^{-1}C}$), LE ($\mathrm{W\,m^{-2}}$), H ($\mathrm{W\,m^{-2}}$) for each source of data. The exploratory metrics are the minimum, mean, maximum, 5_{th}, 25_{th}, 75_{th}, 95_{th} percentiles and standard deviation. The metrics were calculated over the hourly values of both sources.

SOURCE: Own production.

data showed more extreme negative values and a lower maximum value relative to the model. There is better agreement in the mean LE between the two sources. However, above the 95th percentile, the tower data had larger values than the model, indicating that while the tower data do not reach as high peaks as NOAH-MP, the observed data shows a higher frequency of larger values in the distribution (Figure 3.5). This suggests that the overestimation of LE by NOAH-MP shown in Figure 3.2 is caused by the higher frequency of lower positive values by the model, and of negative values in the observed data in the dry season (Figure 3.8). H shows the best agreement between the distribution of data from the two sources among all variables, having smaller differences along all the distribution.

The average diurnal cycle during each season (dry or wet) (Figure 3.8) shows that the observed magnitude of NEE was larger than NOAH-MP during both day and night times. As stated above, this behaviour is more pronounced during the wet season with similar values of NEE during the dry season. The difference between seasons was more pronounced during the day, while during the night there was a small decrease in the observed NEE during dry months. The GPP showed similar behaviour as the negative portion of NEE, being underestimated by NOAH-MP in the wet season, and showing similar values during the dry season. There were large

differences in R_{eco} between the two sources, the NOAH-MP output underestimated the values throughout the day, especially during the wet season. In addition, the model also exhibited a difference in the timing of the increase and decrease of respiration. The LE and H fluxes show better agreement between the two sources, LE show a timing difference in the peak during the day in both seasons, and H was overestimated during wet and dry seasons. It is important to note that H shows better agreement between both data sets during the night time.

Figure 3.8 - Diurnal composites of dry and wet months, showing the average of hourly fluxes from NOAH-MP and flux tower estimates of carbon and energy fluxes.

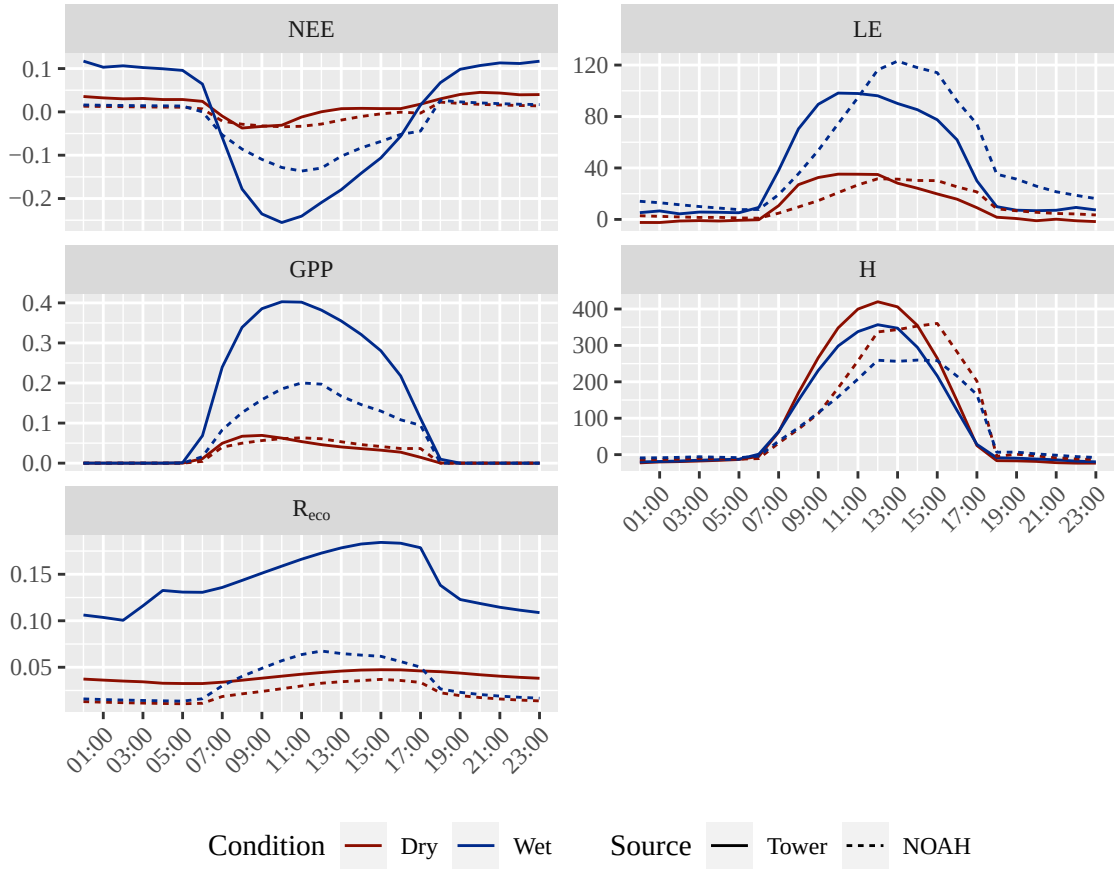

The fluxes are represented as NEE ($\mathrm{g\,m^{-2}\,y^{-1}C}$), GPP ($\mathrm{g\,m^{-2}\,y^{-1}C}$), R_{eco} ($\mathrm{g\,m^{-2}\,y^{-1}C}$), LE ($\mathrm{W\,m^{-2}}$), H ($\mathrm{W\,m^{-2}}$).

SOURCE: Own production.

The modelled values of NEE exhibited a smaller range of values than the observed,

showing a high concentration of values near zero (Figure 3.9). The GPP and R_{eco} also showed a smaller range for NOAH-MP, at some times exhibiting no agreement with observed increases. While the GPP still showed values with a certain level of agreement, the R_{eco} exhibited little agreement between the observations and the model. The LE had a smaller range of observed values, and the scatter plot shows a large variance in values between tower and NOAH-MP values.

Figure 3.9 - Scatter plot of hourly values from NOAH-MP outputs and tower flux derived estimates of carbon and energy fluxes.

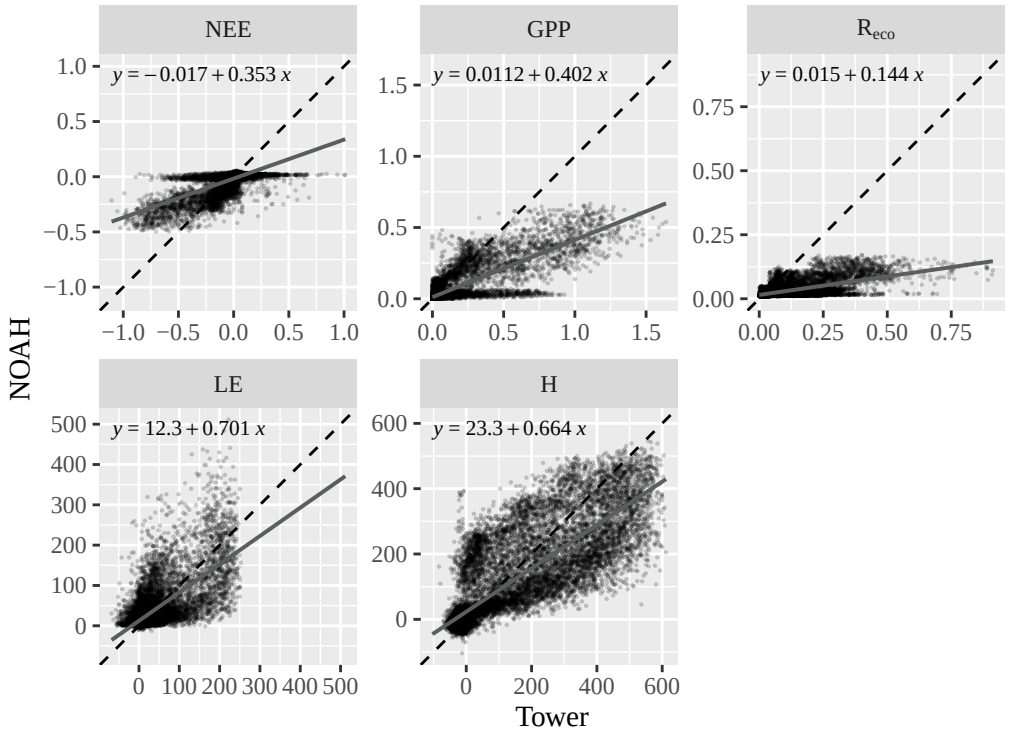

The fluxes are represented as NEE ($\mathrm{g\,m^{-2}\,y^{-1}C}$), GPP ($\mathrm{g\,m^{-2}\,y^{-1}C}$), R_{eco} ($\mathrm{g\,m^{-2}\,y^{-1}C}$), LE ($\mathrm{W\,m^{-2}}$), H ($\mathrm{W\,m^{-2}}$).

SOURCE: Own production.

The modified coefficient of efficiency has a value of $\mathrm{E_1} = 0$ when the modeled values have the same performance as the baseline predictor (in this case the mean) to predict the observed values. When $\mathrm{E_1} > 0$ it is assumed that the model has a better ability to predict than the baseline, and $\mathrm{E_1} < 0$ indicates that the model is worse than the baseline to explain the observed variability (LEGATES; MCCABE, 2013).

The performance of NOAH-MP to predict observed NEE was $E_1 = 0.23$, which means that it could explain 23% of the difference between the observed values and the mean (Table 3.2). As is expected, this value gets lower as the mean monthly, daily and hourly baselines are used, the E_1^m and E_1^d have small decreases, while E_1^d reaches a negative value of -0.06. The use of hourly means for each season exhibits a better predictor than the rest of the estimators. This is expected, since the hourly variations across the days were stronger than the variation from day to day or within the months that are also smoothed by the presence of negative and positive values of NEE, which made E_1^d and E_1^m not much better predictors than the mean in E_1.

Table 3.2 - Model coefficient of efficiency with the use of different baselines along with its components MAD and MAE.

Var	E_1		E_1^m		E_1^d		E_1^h		MAE
	E	MAD	E	MAD	E	MAD	E	MAD	
NEE	0.24	0.09	0.22	0.09	0.19	0.09	-0.05	0.07	0.07
GPP	0.58	0.13	0.44	0.09	0.42	0.09	0.15	0.06	0.05
R_{eco}	0.11	0.07	-0.94	0.03	-2.06	0.02	-0.35	0.05	0.06
LE	0.3	32.74	0.19	28.46	0.15	27.21	-0.13	20.34	23.05
H	0.57	142.68	0.56	140.25	0.55	138.68	-0.49	41.58	62.02

The hourly values from NOAH-MP outputs and flux tower estimates were used to calculate the metrics. Negative values of E means that the baseline is a better predictor than the model.

SOURCE: Own production.

Surprisingly, the GPP showed a much higher E_1 than NEE and R_{eco}, and also resulted in a positive value of E_1^h, even when NOAH-MP showed larger disagreements in GPP at daily and hourly scales in relation to the field observations. This can be caused by a large frequency of zeroes in both sources during the night, which can be contributing to smaller errors in relation to NEE and R_{eco} and can be observed in the MAE values. The E_1^m and E_1^d also don't show a large impact as in E_1^h. This may be due to a similar effect as in the NEE, however it is now caused by the high frequency of zeroes, that tend to smooth the daily and monthly means, decreasing the variation of GPP in these predictors.

The R_{eco} shows the worst performance for NOAH-MP in all analysed variables, and it performs worse at E_1^m and E_1^d than E_1^h. This may be caused by lower variation of R_{eco} in the tower estimates throughout the day, and higher variance at daily

and monthly scales, which better explains the original data. The lack of contrasting values between day and night for R_{eco} (as occurred in GPP, NEE, LE and H), is what makes the daily and monthly means better predictors than hourly means (Figure 3.8).

The LE showed a good agreement in the hourly means for each season (Figure 3.8). However, it resulted in low values of E, having the highest impact on E_1^h, and lower impact from E_1^m and E_1^d for similar reasons as GPP. Although the modeled LE showed a similar response to rainfall as the field observations, the occurrence of rainfall at the daily time scale shows significant differences between both sources (Figure 3.4). When precipitation occurred on different dates, it can cause lower values of E, another possible reason is the significantly higher frequency and magnitude of negative values in the tower data, leading to an increase in the absolute error.

The highest performance values were found for H, which was less impacted by the use of E_1^m and E_1^d predictors as baselines. On the other hand, it was greatly reduced in E_1^h, indicating that the hourly mean better explains the variation of H throughout the time series, and that the model showed its largest errors at this scale, but represents the daily and monthly seasonality well.

The MBE value for NEE points out an overestimation of negative fluxes by the model (Table 3.3). However, if the values of NEE are decomposed into daytime and nighttime, the new values of MBE are 0.002 (smaller negative values) and -0.040 (snaller positive values), respectively. This reinforces that the model is actually underestimating positive and negative NEE, especially positive fluxes during the nighttime. The PBIAS shows that the energy fluxes had the lowest proportional bias, with H having the lowest value (-9.13%). The worse performance of NEE and LE according to NME is due to higher errors in the negative portion of the data, which is neutralized in PBIAS. The SD metric also shows the energy fluxes having the best values, especially LE, that showed similar values of standard deviation from the two sources (Table 3.1).

In summary, the large errors in the NEE estimates by NOAH-MP were found during the wet season, especially in the representation of diurnal variation of fluxes (Figure 3.8). While there were agreements in the monthly seasonality (Figure 3.3), the daily values showed large disagreements in the response of NEE to precipitation (Figure 3.5), where the model showed a slow and smooth response and the field observations respond much more rapidly. These characteristics were also translated into the behaviour of modelled GPP and R_{eco}.

Table 3.3 - Values of other metrics, covering bias, mean error and standard deviation of NOAH-MP outputs and flux tower estimates.

Var	MBE	PBIAS	NME	SD
NEE	-0.02	-18.77	75.91	0.52
GPP	-0.04	-46.52	62.55	0.52
R_{eco}	-0.06	-68.92	71.45	0.76
LE	4.92	17.09	80.06	0.00
H	-11.01	-9.13	51.43	0.20

The metrics were calculated using hourly values from both sources of data.

SOURCE: Own production.

3.4 Discussion

NOAH-MP was suitable in representing the drought impact on energy fluxes (LE and H) at different time scales, based on eddy flux observations. While the model captured the seasonality of the carbon fluxes, it considerably underestimated those, especially during the wet season, even when the model presented a higher annual precipitation than the observations. The annual scale results indicate that the model underestimated the impact of drought for NEE and R_{eco} but represented it well for GPP, although its absolute values were considerably smaller than the tower data. At the daily scale, the major discrepancies between model output and field observations were the response of carbon fluxes to rainfall in a short term.

It is not clear what is causing this behavior in NOAH-MP. Some of the main limitations in state of the art LSMs in simulating the vegetation response to drought is in the representation of stomatal conductance (g_s) and apparent maximum carboxilation rate (Vc_{cmax}) to decreasing water availability (ZHOU et al., 2019). A possible limitation of NOAH-MP is the static parameter of Vc_{max}, which is fixed as 40 $\mu mol\, m^{-2}\, s^{-1}$ for open shrublands. A study conducted in the same area in 2013 and 2014 calibrated values of Vc_{max} for 11 native species representative of that area showed values ranging from 10.7 to 123.2 $\mu mol\, m^{-2}\, s^{-1}$. After the implementation of the equations in the Integrated Model of Land Surface Processes (INLAND), Rezende et al. (2016) noticed a considerable improvement in the estimations of NEE and GPP. Although it is important to note that even in the uncalibrated model run conducted by Rezende et al. (2016), the model was successful in representing the fast response of GPP and NEE following rainfall events, which NOAH-MP failed

to represent in this case. Kauwe et al. (2015) tested different drought sensitivities in the Community Atmosphere Biosphere Land Exchange (CABLE), based on different Vc_{max} and g_s according to environmental factors. They noted that different drought sensitivities improved CABLE's simulation of LE and GPP over xeric sites, which shows abrupt decline of those variables during the dry period. In other words, it overstated the impact of drought in these sites, as they show less sensitivity to water limitation, taking longer to show a decrease in LE and GPP. This is not the case for the Caatinga site analysed in this study, where it is possible to observe this rapid decline after the rainy season, and also a fast recovery even with small amounts of rainfall, while NOAH-MP shows slower decline of GPP and LE.

The comparison of the LE between the two sources of data shows low values of performance metrics. However, the model shows a better agreement with its response to rainfall (Figure 3.5), that is an abrupt increase of latent heat following precipitation. Even though the LE has a relationship with vegetation activity, it is not translated into the GPP estimates in NOAH-MP, as occurs in the field observations. It is worth noting that while H and GPP showed the best values of E, both of these variables show high levels of agreement during night time (Figure 3.8). This is especially true for GPP, since both sources show values of zero during the period, which lowers the value of MAE in relation to MAD, causing better values of E. However, since the night time values of GPP are zero in both sources, there are no estimates to be made during this period. In other words, it is not a merit of the model to reach this agreement with tower data, making the performance index biased in favor to the model output. This highlights the importance of exploring the nature of each variable when validating models, since the evaluation based only on performance indices can be flawed in some cases. The use of other metrics and time series plots are essential to assess model performance. If we analyse the values of E for GPP taking the zeros out of the analysis, the new values of E_1, E_1^m, E_1^d and E_1^h would be 0.488, 0.042, -0.034 and 0.157, respectively. Surprisingly, the high value of E_1 is maintained, which is most likely caused by the high agreement in GPP estimates during the dry season, where there is not a significant amount of variation. However, when the baseline shows the slightest change above the hourly scale (E_1^m and E_1^d), the performance of the model drops, specially for E_1^dm reaching negative values, which reinforces the lack of capability of the model to represent variations between days in GPP. These observations reinforce the importance of using baselines to assess model performance, as it is done in Best et al. (2015). By using conceptual models and regressions as baselines, we can avoid over estimations of model performances.

3.5 Conclusions

The NOAH-MP simulated LE and H fluxes showed the best performance compared to the observations. Modeled LE showed good agreement with field data with respect to the relationship between LE and precipitation. The modeled carbon fluxes showed lower performance, while it was able to represent well inter- and intra-annual variations seen in the field observations. The daily and hourly fluxes showed a lack of capacity of the model to represent the short term relationship between carbon flux and precipitation.

We have shown that the use of performance metrics are essential in assessing the performance of the model is an ecosystem that is not well understood. While there are areas of needed improvement, this research illustrates a step towards understanding the dynamics of water and carbon cycling in an area that may be profoundly impacted by future climate change.

4 MODELLING ECOSYSTEM RESILIENCE TO DROUGHTS: ASSESSING THE ESTIMATION OF RESILIENCE BY MULTIPLE SIMULATIONS OF PRECIPITATION REGIME

4.1 Introduction

The concept of how ecosystems will be affected by climate change has been given more attention over recent years, being key to exploring elements present in the IPCC reports, such as the impacts, adaptation, mitigation and vulnerability induced by climate change. One concept that might be used to characterize this is the concept of engineering resilience (henceforward referred to as resilience in this paper), which is commonly associated with other concepts, such as resistance, impact, recovery and stability. There is a wide range of definitions for the concept of resilience (LAKE, 2012), which can be more specific, as being the rate of return of a system to its equilibrium state after a disturbance (MACGILLIVRAY; GRIME, 1995; KEERSMAECKER et al., 2014), or more broadly, as being the capacity of the system to maintain its function under the effect of exogenous disturbances (HODGSON et al., 2015; HOLLING, 1973; WALKER et al., 2004). The quantification of resilience is a challenge and the comparison between different systems is difficult. This is due to the fact that there are many variables involved including: the nature and severity of the disturbance (RATAJCZAK et al., 2018), the variables used to indicate the systems state, the metrics used to quantify the resilience (INGRISCH; BAHN, 2018), and the state and quality of the data gathered (KEERSMAECKER et al., 2014). There is a need for developing systematic ways of estimating resilience (INGRISCH; BAHN, 2018), and the use of long term and spatially extensive data along with manipulation of disturbance drivers can help improving the understanding and estimating resilience (RATAJCZAK et al., 2018; INGRISCH; BAHN, 2018; NIMMO et al., 2015).

In this study we follow the recommendation of Hodgson et al. (2015) who suggest that since the resilience is assumed to have many interpretations that we should use the broadest definition possible. Therefore, we assume that the definition of resilience is characterized by the quantification of its components, which are the impact (which is the inverse of resistance) and recovery. We also adopt a measure of stability that would be affected by both of these components. We also assume that a system is a combination of climatic and vegetative characteristics (other variables could be added, but for simplicity, we will focus solely on vegetation and precipitation), and that a disturbance is an abnormal event with negative impacts within the system (e.g. vegetation productivity) caused by a driver (e.g. precipitation). The impact

would be the negative change in the system, caused by the driver, and the recovery would be the positive changes caused by the systems driver following the impact as the system returns to a normal state. This assumes that a stable or normal state of the system exists. The resilience of a system would be the characterization of how the system responds to the integrated relationship between drivers and state variables, which would be characterized as a function (not a single value).

The objective of this study was to explore the estimation of resilience components for different vegetation types by manipulating the precipitation regime through simulations performed by the Noah-Multiparameterization Land Surface Model (NOAH-MP). We hypothesize that the resilience of an ecosystem is a function of intrinsic characteristics of this ecosystem with climatic conditions. Here we will use a land surface model (LSM) to assess how different vegetation types differ in their resilience to drought. We believe that this will result in a function of how resilience changes under different environmental conditions.

4.2 Material and methods

4.2.1 Study area

In order to assess the ecosystem resilience to drought, we will examine the Caatinga biome. The study area covers an extent of approximately 10000 km^2 between the coordinates 9.65°S, 40.8°W and 8.77°S, 40.0°W (Figure 4.1). It is located in the semi-arid region of northeast Brazil, more specifically the western portion of the Pernambuco (PE) state and the northern region of the Bahia (BA) state, and includes the cities of Petrolina (PE), Lagoa Grande (PE) and Juazeiro (BA).

This area is inserted within the meridional sertanean depression ecoregion inside the Caatinga, which occupies most of the central and southern regions of this biome and presents the most characteristic landscape of the northeast semi-arid region (VELLOSO, 2002). The study area is estimated to have 60.5% of the area impacted by human activities (SILVA BARBOSA, 2017). The predominant and most characteristic vegetation formation of this region is the Crystalline Caatinga, classified as Seasonally Dry Tropical Forest and Woodlands (SDTFW), composed mostly by shrublands, spiny woodlands and small forests (QUEIROZ et al., 2017). The predominant soils in the study area are deep argisoils and latossoils in the northern side of São Francisco river, and shallow planossoils in the southern side.

Figure 4.1 - Location of the study area in the Brazilian territory, meteorological stations and flux tower, accompanied by the total annual precipitation time series.

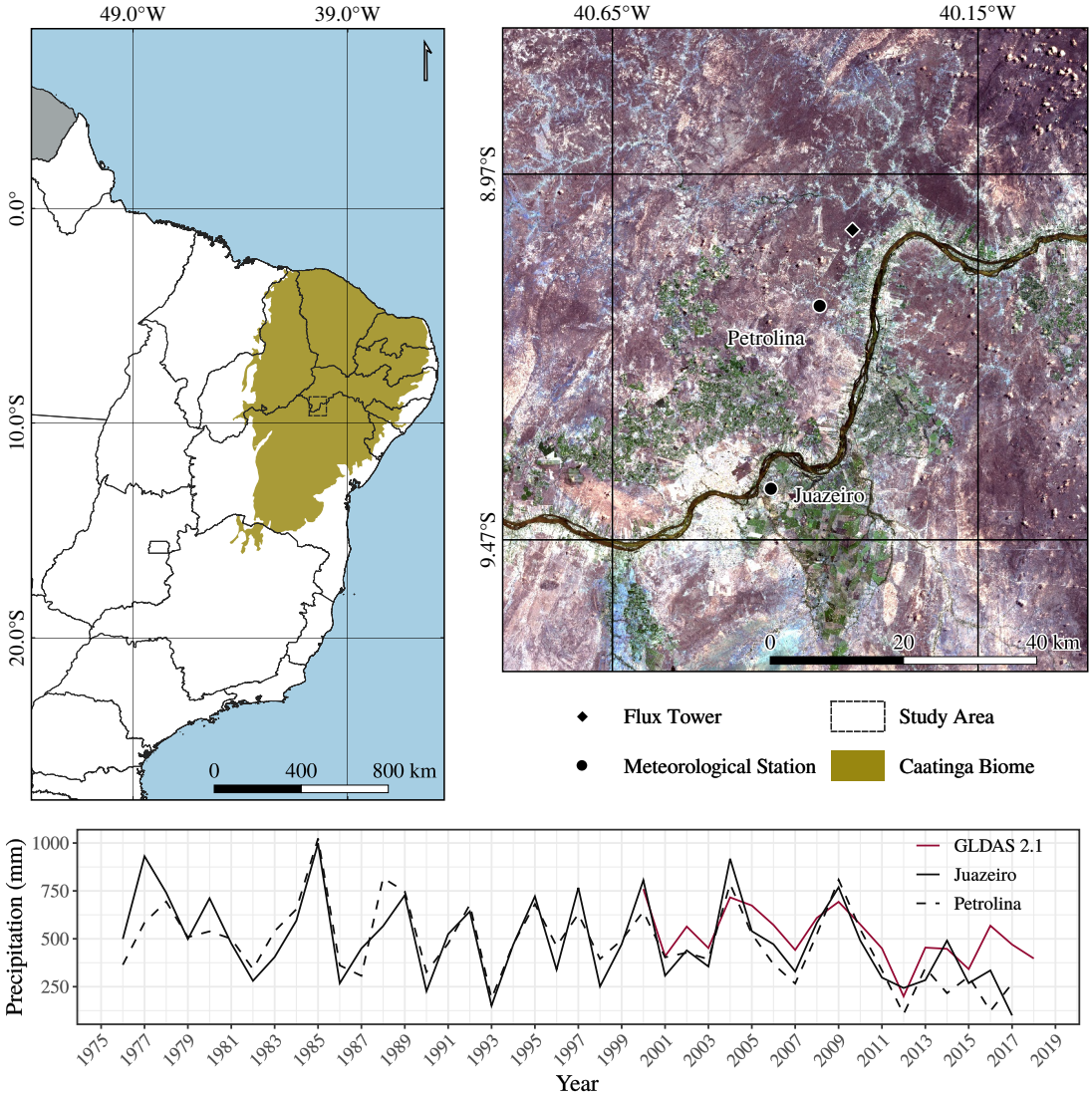

The annual precipitation was measured by meteorological stations and estimated by the Global Land Data Assimilation System (GLDAS 2.1). The satellite image is a true color composite, derived from Sentinel 2 collection from 21/09/2019.

SOURCE: Own production

According to the MODIS land cover product (MCD12Q1) collection 5, most of the area is occupied by open shrublands, savanna and woody savanna (Figure 4.2). There are also smaller patches of grasslands and closed shrublands. The different land cover types have different parameter values assigned to each in NOAH-MP, and

is what differs vegetation types from each other.

Figure 4.2 - Distribution of land cover types in the study area.

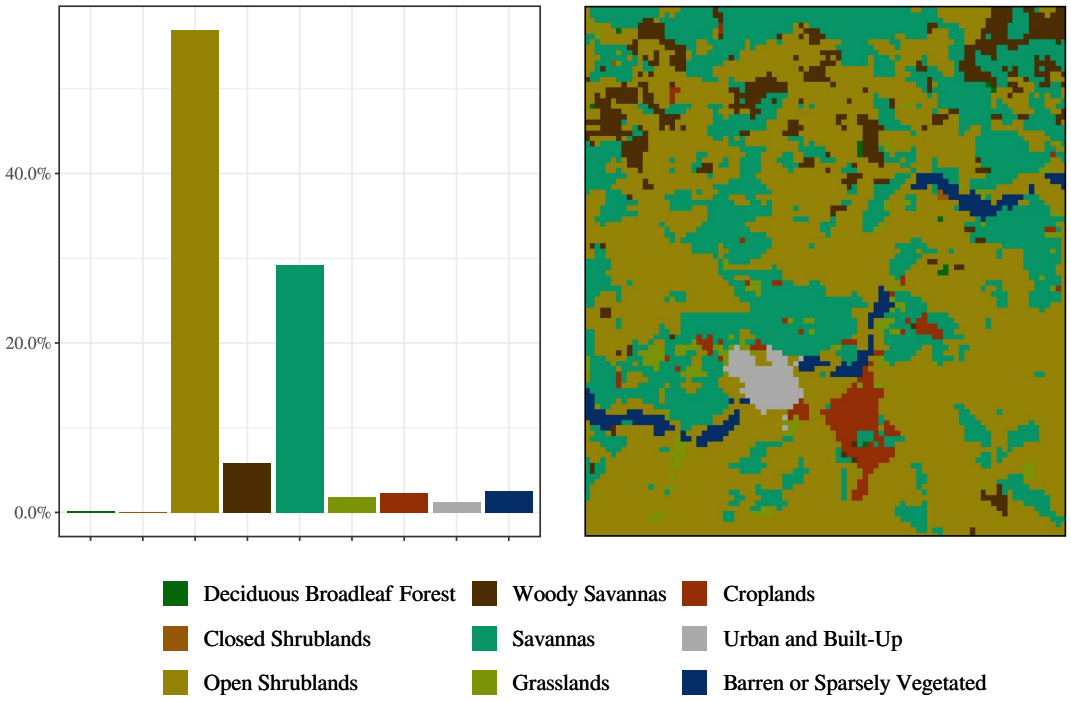

The land cover was extracted MODIS MCD12Q1, collection 5, following the IGBP classification scheme

SOURCE: Own production.

4.2.2 NOAH-MP

The vegetative response to drought was assessed using the NOAH-MP land surface model. The NOAH-MP is an improved version of NOAH-LSM, including multiple options to parameterize the vegetation canopy surface energy balance, frozen soil and snow, groundwater interaction with soil, surface runoff and ground water discharge, and vegetation dynamics (NIU et al., 2011).

The model was configured to run with a spatial resolution of 1km, in a grid of 99 x 99 cells. The scale and resolution were defined based on a balance between computational cost, representativeness of the region, and the ability of distinguishing the different land cover types within the study area.

We utilized the NASA Global Land Data Assimilation System (GLDAS) data for meteorological forcing, with a spatial resolution of 0.25 degrees every three hours (RODELL et al., 2004). The GLDAS forcing data were interpolated to intervals of one hour to run NOAH-MP.

The dynamic vegetation was parameterized using the maximum fractional vegetation, which uses a Ball-Berry type stomatal resistance. We used the NOAH formulation for the soil moisture factor controlling stomatal resistance. The adopted run-off and groundwater scheme were the TOPMODEL with simple groundwater, the surface exchange coefficient for heat was based on Monin-Obukhov similarity theory, and the radiation transfer was represented by a two-stream scheme for the vegetated fraction. More details of the the option schemes are described in Niu et al. (2011).

The land cover dataset adopted in the model runs is the MODIS MCD12Q1 product collection 5 (FRIEDL, 2015). The classification of the land cover in the extracted cell, where the flux tower is located, is open shrublands, according to the MCD12Q1 product following the IGBP classification scheme.

4.2.3 Generation of precipitation forcing scenarios

The model was forced with precipitation scenarios of different magnitude and duration of drought. The scenarios consisted of a normal period followed by a drought period of varying magnitude and duration, then consisting of a return to a normal or wet period of varying magnitude and duration. This was done in order to more fully capture the range of possible responses to precipitation variability in the region.

The precipitation scenarios were defined in relation to the precipitation measured at the meteorological stations within the study area and the GLDAS precipitation data (4.1). We analyzed the historical precipitation (1975 - 2017) to statistically define which years would be considered as "Dry", "Normal" or "Wet", according to their annual precipitation. In order to capture the range of precipitation variability, we further define three cases of "Dry" (D1, D2 and D3) and three cases of "Wet" (W1, W2 and W3) based on the quantiles of annual precipitation. This results in seven (3 dry, 3 wet and 1 normal) years to construct the precipitation scenarios.

In order to determine the actual years of precipitation data to construct the scenarios, we used a quantile approach. The classification of years were based on quantiles of the observed station data compared to the GLDAS data, divided in the three

classes: dry years are represented between the 0.05 and 0.40 quantiles, normal years between 0.40 and 0.60, and wet years between 0.60 and 0.95. We then extracted the minimum, mean and maximum values of annual precipitation from wet and dry years, and the mean of the normal years. From the distribution of the annual precipitation (Figure 4.3), we selected the years of data from GLDAS 2.1 that most closely matched the quantile amounts to generate the precipitation forcing scenarios (Table 4.1). The obtained classes of years were named as D1, D2 and D3 for dry years, N for normal years, and W1, W2 and W3 for wet years.

Figure 4.3 - Distribution of the annual precipitation and the classes of years.

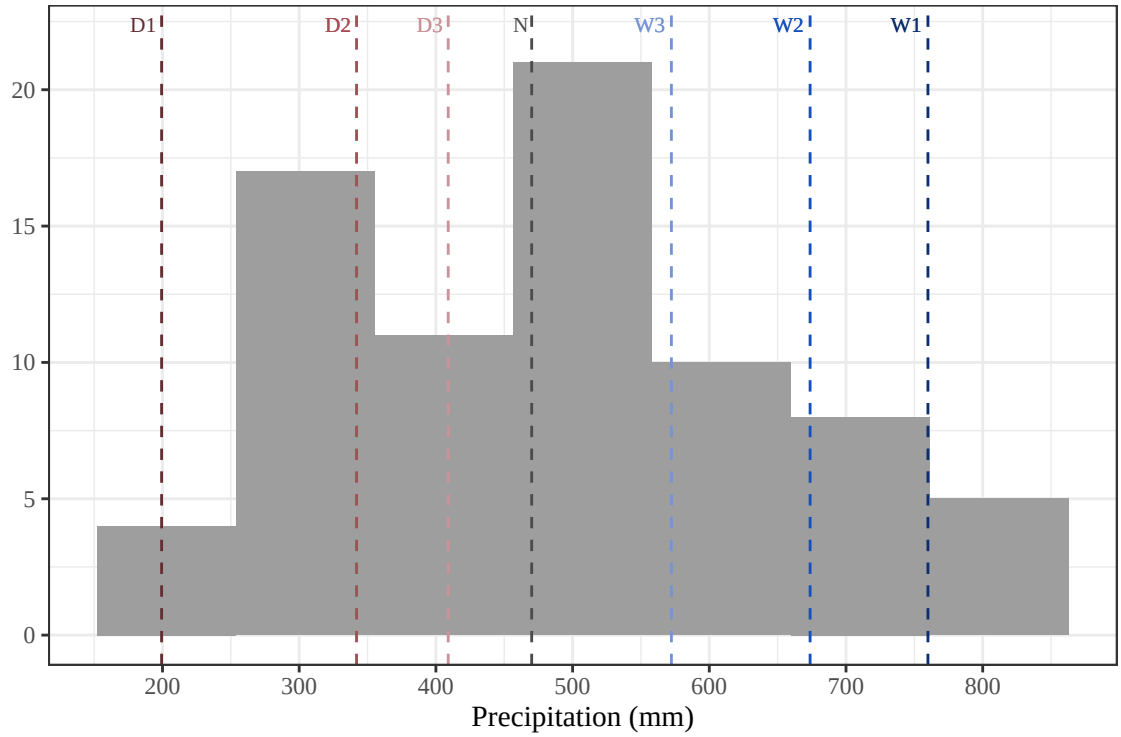

The histogram is based on the historical series of annual precipitation measured by the meteorological stations of Juazeiro and Petrolina (grey bars). The vertical dashed lines represents the annual precipitation of years selected for each class.

SOURCE: Own production.

In order to create the scenarios, we created 49 sequences of 13 years from each precipitation class, consisting of three stages to represent a situation of disturbance and recovery. Each scenario begins with a sequence of five normal years (N) in

Table 4.1 - Years selected for each class from GLDAS 2.1.

Class	Year	GLDAS	Stations	Metric	Quantile
D1	2012	199.36	216.30	Min	0.00
D2	2015	341.96	316.74	Mean	0.26
D3	2001	409.03	404.60	Max	0.38
N	2017	470.07	478.77	Mean	0.45
W3	2006	572.26	524.40	Min	0.72
W2	2005	673.74	653.45	Mean	0.83
W1	2000	759.95	808.40	Max	0.93

The classification were based on annual precipitation from the meteorological stations measurements. The selection of years were made in function of the proximity between GLAS 2.1 estimates and the stations measurements, as also the agreement over the intra-annual precipitation regime.

SOURCE: Own production.

order to account for spin-up and develop an equilibrium to the normal precipitation regime. The second stage represents the disturbance event, which was composed of a sequence of dry years (D1, D2, D3) ranging from one to four years of drought. The third stage represents the recovery period, in which we used a sequence of four normal or wet years (N, W1, W2, W3). This results in a suite of 49 scenarios representing a range of drought intensity and magnitude as well as a range of possible recovery (Figure 4.4). These scenarios were then used to provide forcing data to run NOAH-MP.

4.2.4 Data analysis

In order to estimate the resilience and its components, we followed the methodologies proposed by Ingrisch and Bahn (2018) and Lloret et al. (2011). These approaches are based on the determination of several indices representative of the pre-disturbance state (s_0), the disturbance impact (s_i) and the post-disturbance (s_r). In this study, we are interested in multiyear droughts. Therefore, we constructed scenarios in which we have one or more years of drought. This requires that we also take in account the full impact of the reduction in productivity by including a second value of impact ($s_{i'}$). This allows for consideration that the impacts on the recovery estimation due to fact that the response will likely to change with the temporal extent of the drought. We characterize the drought by the annual precipitation and the duration in years. The resilience analysis was based in annual sums of the analysed variable, as is described in Figure 4.5.

Figure 4.4 - Scenarios characterization scheme.

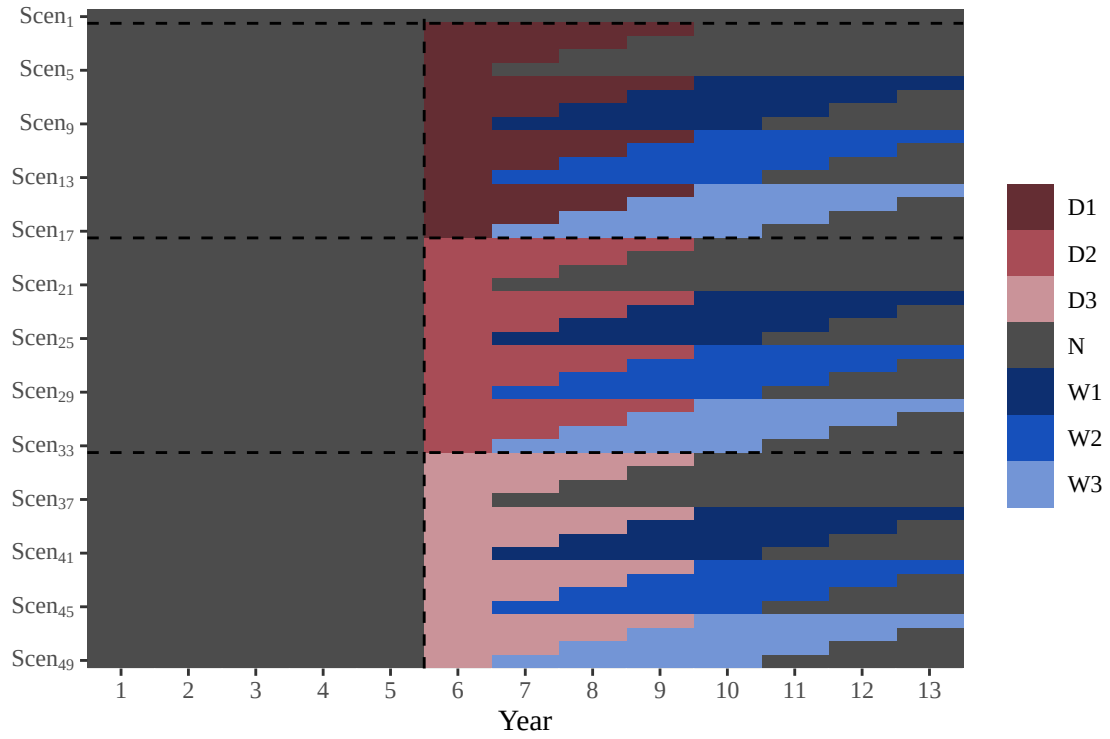

The sequence of years of different classes composing each scenario, with an additional scenario in which every years were normal years ($Scen_1$). The different combination of years generated a total of 49 different scenarios.

SOURCE: Own production.

Next, we extracted the values of each of the indices from Figure 4.5 for each cell of each scenario. The extraction of s_0 is simply the value of the year 5 (the last normal year before the disturbance), s_i is the value during the year with the lowest state during the disturbance period, with the condition $s_i < s_0$, $s_{i'}$ is the value during the last year of the disturbance, and s_r, is the value extracted from the first year when $s_r > 0.95 * s_0$. We only considered situations where $s_i < 0.90 * s_0$ (an impact larger than 10%), were to be considered as a disturbance, and hence would be included in the estimation of the resilience components.

In the literature there is a wide variety of formulas used to calculate resilience and its components, which will also have an effect in the final results. In this study we decided to use simple metrics to calculate the resilience components, impact, recovery, and stability. All metrics used are dimensionless, facilitating the comparison

Figure 4.5 - Representation of drought impact and recovery for resilience estimation using annual values.

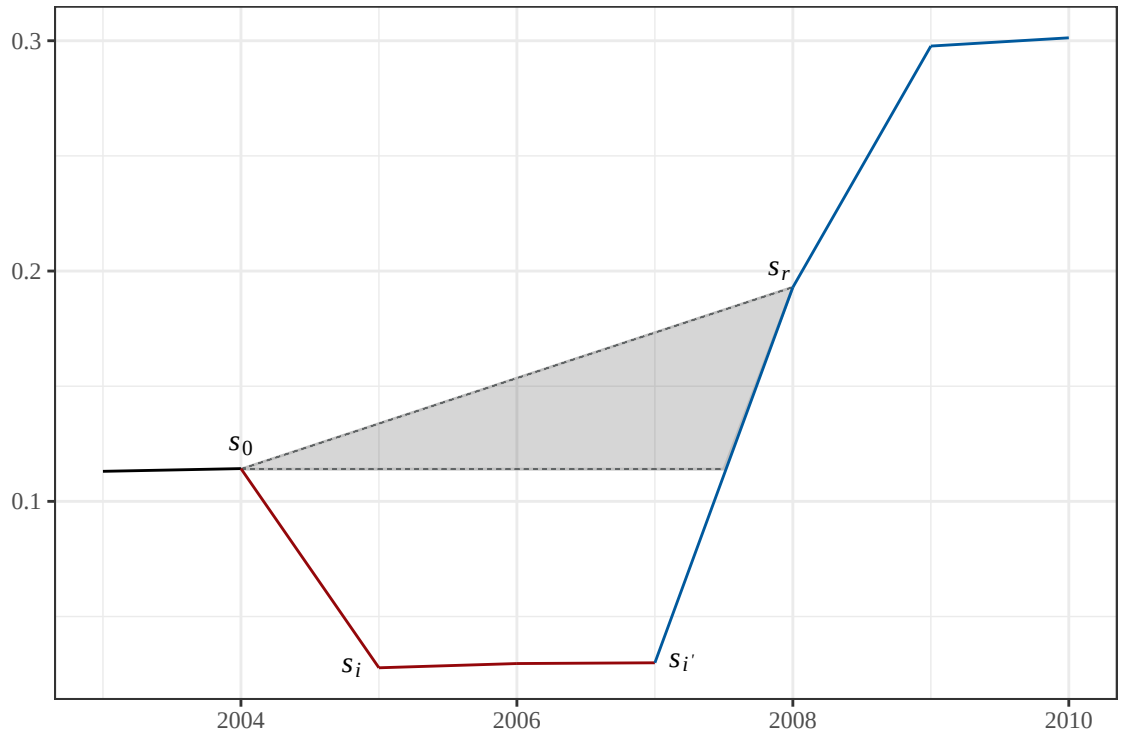

The scenario 07 (D1-W1-2) was used to generate the figures. The dotted lines and the gray shaded areas represent the condition when the system state surpassed s_0 (bottom dotted line), however, by using annual values, the recovery will be accounted for the sum of the year in which the system state is higher than s_0 (upper dotted line).

SOURCE: Own production.

between different variables, events and regions. The impact and recovery metrics were based on formulas proposed by Ingrisch and Bahn (2018), and the stability metrics is based on the coefficient of variation (KEERSMAECKER et al., 2014; ZANG et al., 2014; SCHEFFER et al., 2015; GAZOL et al., 2016).

Using the indices from Figure 4.5 we can quantify the following metrics. The impact of the disturbance is:

$$Impact = 1 - \frac{s_i}{s_0} \tag{4.1}$$

The baseline normalized recovery is calculated as:

$$Recovery_{base} = \frac{s_r - s_{i'}}{s_0} \tag{4.2}$$

The impact normalized recovery is calculated as:

$$Recovery_{impact} = \frac{s_r - s_{i'}}{s_0 - s_i} \tag{4.3}$$

The stability is quantified as:

$$Stability = \frac{\sigma}{\mu} \tag{4.4}$$

where σ and μ are the standard deviation and the mean calculated from the time series for each scenario.

Each metric was calculated by using annual values of gross primary productivity (GPP) and precipitation. For GPP, the metrics will be named in the same manner in the equations cited above ($Recovery_{base}$, $Recovery_{impact}$, $Impact$ and $Stability$), for precipitation new names were given ($Precipitation\ Increase_{base}$, $Precipitation\ Increase_{impact}$, $Precipitation\ Impact$ and $Precipitation\ Stability$, respectively).

In order to analyse the differences between vegetation types, the data was filtered, using the model grid cells of only one soil type present in the area of study (the most predominant), classified as sandy clay loam (soil type number 7 in NOAH-MP). This was performed in order to avoid that the results would also be affected by different soil types.

The analysis was conducted by exploring the indices representing various components of the resilience. These include the $Recovery_{base}$, $Precipitation\ Increase_{base}$, $Recovery_{impact}$, $Precipitation\ Increase_{impact}$, $Impact$, $Precipitation\ Impact$, $Stability$, and $Precipitation\ Stability$. In order to assess the ecosystem responses to precipitation variability, we focus on the gross primary productivity (GPP) as the primary variable to assess the impact of the drought in order to visualise possible differences in the resilience components across vegetation types.

To test the significance of these differences, we implemented a sub-sampling scheme for each land-cover type. We randomly selected 400 points from each scatterplot and repeated this process 10000 times. For each 400 point sample, we calculated a lin-

ear regression for the GPP components as a function of precipitation components. This facilitates analysis of the effect of precipitation variation on GPP in each scenario by giving us more confidence in the regression parameters. We then calculated the difference for each vegetation type, considering a 95% confidence interval. This method was chosen in order to avoid the potential effects of dependency due to the spatial correlation between nearby cells and across scenarios.

We also analysed the dispersion between GPP and precipitation components, followed by an analysis using the same sub-sampling method described above, but applying linear regressions for each iteration, and calculating the 95% confidence intervals for the regression coefficients. Finally, we analysed the relationship between the two recovery components and the impact component in order to explore how the different indices impacted the estimated recovery of a system. This sequence of analyses were done in order to explore a methodology to analyse differences in resilience components across different vegetation types, and taking advantage of the capacity of NOAH-MP to simulate water, energy and carbon cycles, and to generate a high number of different scenarios, forming an experimental dataset that can simulate real world processes.

4.3 Results

A preliminary analysis showed little changes in relation to the scenarios with two or more consecutive dry years, increasing the amount of redundant information. Therefore, data of the scenarios with more than two consecutive dry years were discarded, so only half of the scenarios were used to analyse the data.

The range of values estimated for each resilience component presents a large variation along the area for the scenarios (Figure 4.6). The $Recovery_{base}$ ranges from 0 to 3.3, in which most of the values are below 1 (see the third quartile in Figure 4.6). The differences between the mean and median of vegetation types are subtle, higher differences can be observed in extreme values above the fourth quartile. The $Precipitation\ Increase_{base}$ shows a smaller range of values than $Recovery_{base}$, (from 0 to 1.9), also the values under the third quartile are lower than the values found for $Recovery_{base}$, which indicates that smaller variations of precipitation lead to higher variations of GPP for these vegetation types. We can also note that differences in the quartiles between vegetation types are similar for $Precipitation\ Increase_{base}$ and $Recovery_{base}$. The $Recovery_{impact}$ and $Precipitation\ Increase_{impact}$ show a large range of values from 0 to 12.4, with values concentrated under 2.5. As the baseline normalized recovery components, the impact normalized recovery shows similar be-

havior with the increase of precipitation (also normalized by its decrease), but, in this case, there is a vegetation type (Woody Savannas) that shows a clear difference in extreme values in relation to the others. The *Impact* and *Precipitation Decrease* ranges from 0.10 to 0.93, and also shows smaller values of *Precipitation Decrease* than *Impact*, which suggests also that a smaller decrease of precipitation causes a higher decrease of GPP. The *Stability* and *PrecipitationStability* ranges from 0.04 and 0.82, and, like the other components, show higher values for components calculated from GPP.

The result of the difference between the median of the ratio of GPP and the precipitation components of each vegetation type using multiple random sub-sampling technique (Figure 4.7) shows that there are significant differences between at least two vegetation types for all the resilience components. It is possible to observe that the results from $Recovery_{base}$ and $Recovery_{impact}$ are different from each other, although both represent the same component of resilience. We can also note that for some comparisons, $Recovery_{impact}$ and $Impact$ shows a positive feedback, for example, woody savannas shows a higher $Recovery_{impact}$ and smaller $Impact$ than savannas, grasslands and open shrublands. The *Stability* shows a result more similar to $Recovery_{base}$ and $Recovery_{impact}$ than $Impact$, since the *Stability* represents the variation of the variable with time (the higher the score, the higher the variation). This suggests that in this case it is more affected by the recovery component than the impact component of Resilience. This is plausible since the structure of the scenarios introduced more variation in the Recovery than the Impact component.

The median of the ratio of GPP components and precipitation components shows differences between the vegetation types. However, it is also possible to analyse the relationship between GPP and precipitation components with regressions, which gives information about how the vegetation responds along a gradient of different precipitation regimes. The relationship between GPP and precipitation components describes how the vegetation responds to droughts and its posterior recovery (Figure 4.8).

Figure 4.6 - Boxplots of resilience components for each vegetation types.

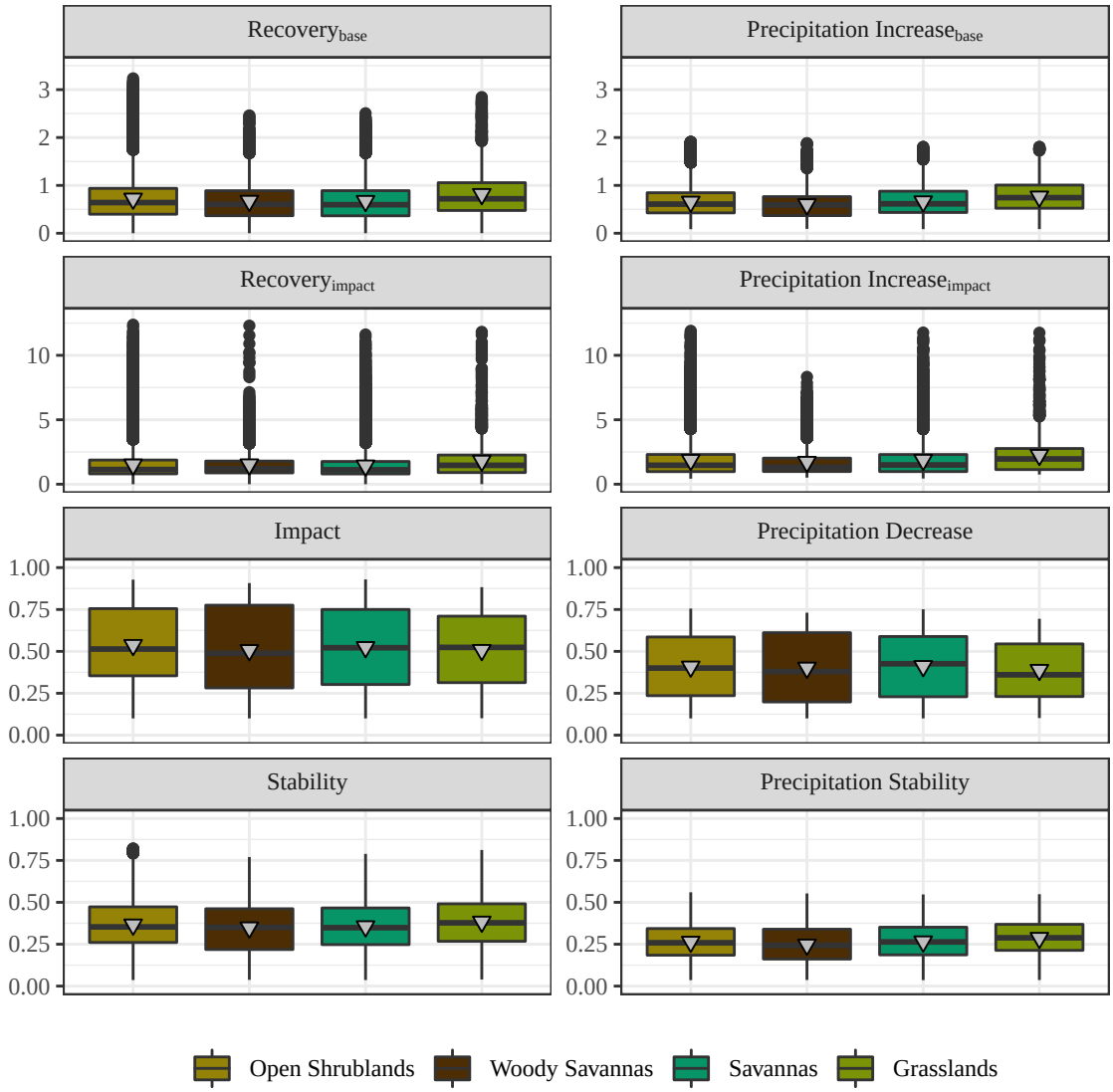

The boxplots were generated for GPP (left side) and precipitation (right side) for each vegetation type. The solid line inside the box represents the median, and the inverted gray triangles represent the mean.

SOURCE: Own production.

The relationship between $Recovery_{base}$ and $Precipitation\ Increase_{base}$ shows that the overall increase of GPP after disturbance is higher than the increase of precipitation. In other words, a smaller increase of precipitation causes a higher increase of GPP, while for $Recovery_{impact}$ and $Precipitation\ Increase_{impact}$ this characteristic is not clear. It is possible to observe that there is a larger variance of points in the

Figure 4.7 - Differences between the median of the factor of GPP components and precipitation components.

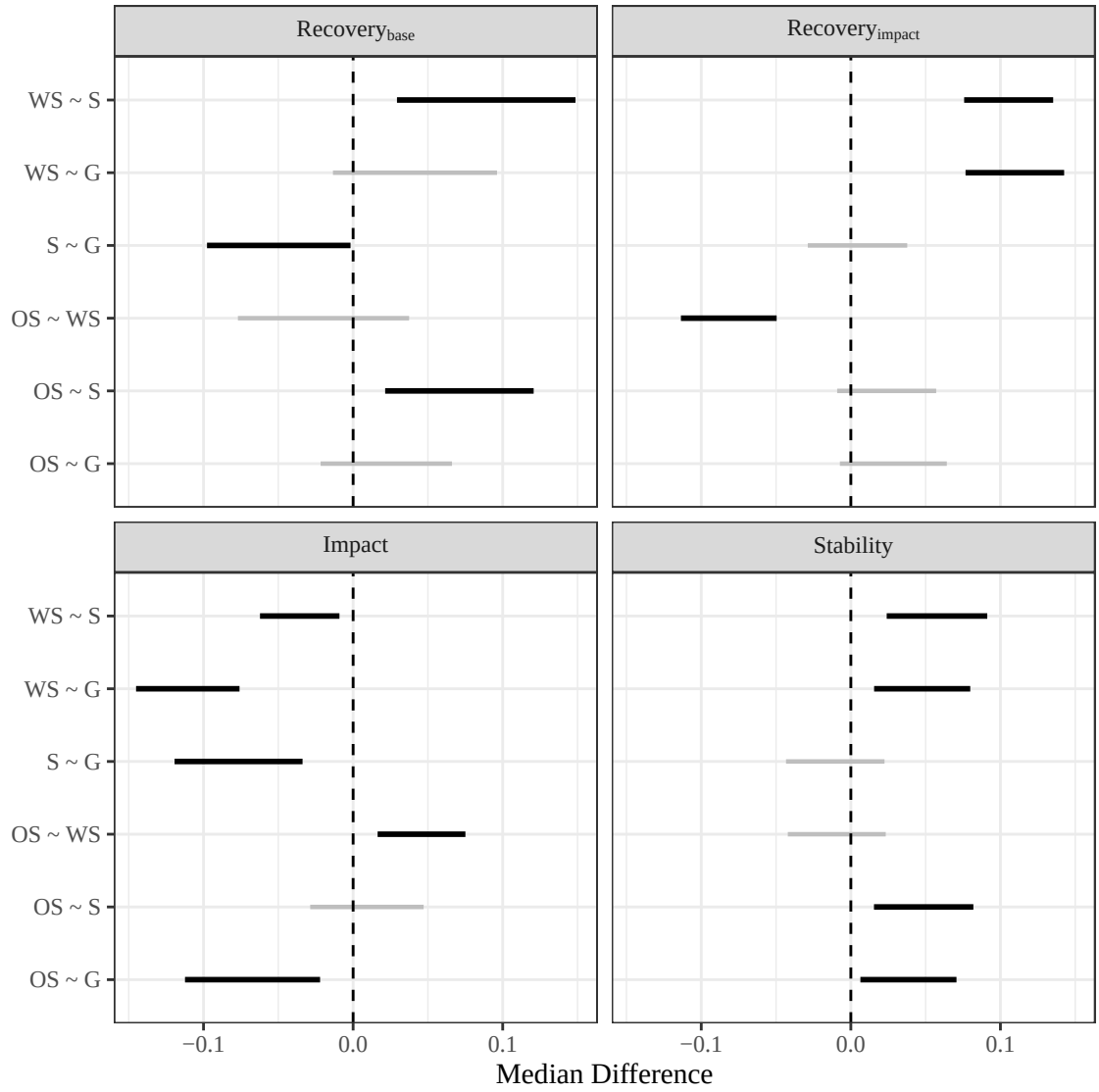

The horizontal solid lines represents the 95% confidence interval of the difference between the range of medians estimated by a sub-sampling procedure, in which gray lines represent non significant differences, and black lines represent significant differences between vegetation types. The vertical dotted lines represents difference = 0, which indicates whether there is evidence or not to reject the hypothesis that the differences are not significant. The vegetation types are represented by abbreviations: Open Shrublands (OS), Woody Savannas (WS), Savannas (S), Grasslands (G).

SOURCE: Own production.

scatter plot, and a high concentration of points in a region close to 1, and it shows a tendency for these points to be under the 1:1 line, which indicates a smaller sensitivity of GPP to precipitation increase, which diverges from the results obtained from baseline normalized components. It is also worth noting that the use of medians of the factor between GPP and precipitation components found significant differences between vegetation types (Figure 4.7).

Assessing the relationship between the $Recovery_{impact}$ and $Precipitation\ Increase_{impact}$ is appropriate with median estimates, since the scatterplot has a high concentration of paired observations within a small range of values 4.8). The $Impact$ and $Precipitation\ Decrease$ shows a somewhat non linear relationship, where the impact over GPP is more sensitive to Precipitation decreases, so small decreases of precipitation causes higher reduction in GPP. In the case of $Stability$ and $Precipitation\ Stability$, there is a more linear relationship, with a higher sensitivity of GPP to precipitation, which means that GPP is less stable than Precipitation in this system.

By performing a simple linear regression for each iteration of the random sampling of each vegetation type, we created an interval of possible regressions between GPP and precipitation components for each vegetation type (Figure 4.9). The regressions can help explain different relationships between GPP and precipitation for each vegetation type in a gradient of precipitation regimes. This will be characterized by the intercept and slope of the linear regression, explaining the effect of precipitation effect over the system state (GPP) from low to high precipitation variations (impact or recovery). The regressions of $Recovery_{base}$ and $Precipitation\ Increase_{base}$ show that the different vegetation types have a similar behaviour in general. It is possible to observe that all of them have less GPP sensitivity to precipitation increase (values under the dotted line) in lower values close to 0. They all exhibit increased sensitivity to precipitation increases (values above the dotted line) at higher values. There are subtle but significant differences between vegetation types, especially in the case of savannas which present less sensitivity to higher precipitation increases. Grasslands show less sensitivity to lower precipitation variations, and higher sensitivity to higher precipitation variations.

Figure 4.8 - Dispersion between GPP and precipitation components.

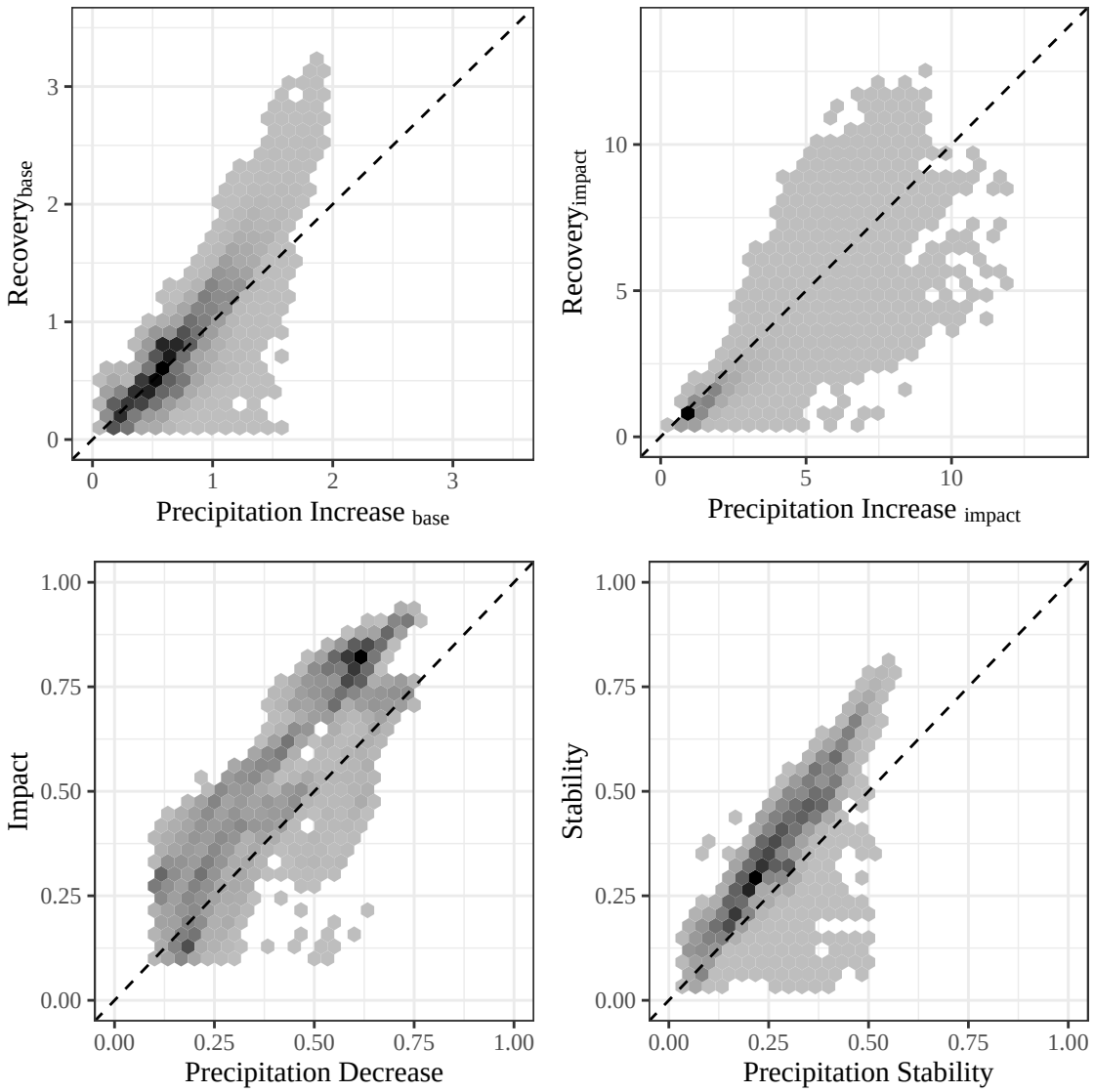

Gray hexagons represent areas with less concentration of paired values, black hexagons represent areas with a higher concentration of points. The diagonal dotted line represents the 1:1 line.

SOURCE: Own production.

Surprisingly, the relationship between $Recovery_{impact}$ and $Precipitation\ Increase_{impact}$ shows a divergent result in comparison to the baseline normalized components, in this case, the regressions point to a smaller sensitivity of GPP to precipitation increase, in which the most discernible differences are shown for woody savannas, with higher sensitivity to precipitation, and

savannas with lower sensitivity.

It is worth noting that the scatter plot of $Recovery_{impact}$ and $Precipitation\ Increase_{impact}$ from Figure 4.8 shows a high concentration of paired values, and possibly are not as appropriate to be analysed by a regression in comparison to $Recovery_{base}$ and $Precipitation\ Increase_{base}$, which clearly shows a line shaped dispersion.

The regression between $Impact$ and $Precipitation\ Decrease$ shows larger differences for savannas and woody savannas in comparison to grasslands and open Shrublands. The first two show reduced sensitivity of GPP to smaller precipitation decreases, and higher sensitivity to larger precipitation increases. In the case of $Stability$ and $Precipitation\ Stability$, the differences between vegetation types are very subtle for all values of $Precipitation\ Stability$, which shows that GPP is less stable than the precipitation (more variation of precipitation means even more variation in GPP). This corroborates the results from the baseline normalized recovery and impact components, that show an increasing sensitivity of GPP as variation of precipitation gets larger. The linear regressions were used to perform an exploratory analysis of the relationships between GPP and precipitation variations. However, by analysing the residual histogram and dispersion, it is possible to observe that the relations may be non linear, which suggest an increased complexity of these relations.

By testing the differences of the coefficients of the linear regressions, it is possible to estimate the significance of these differences (Figure 4.10). The intercept represents the variation of GPP when the variation of precipitation is zero, which can be useful to analyse the effect of low variations of precipitation over the GPP. So the lower the intercept, the smaller the sensitivity of GPP to low precipitation variations. The slope represents the evolution of the GPP sensitivity as the variation of precipitation gets higher. Therefore a slope greater than one indicates that the vegetation shows a higher sensitivity as the larger the variation in precipitation. A slope less than 1 indicates that the effect of precipitation variation over GPP gets smaller as the precipitation gets larger.

Figure 4.9 - Linear regressions between GPP and precipitation components of resilience for each vegetation type.

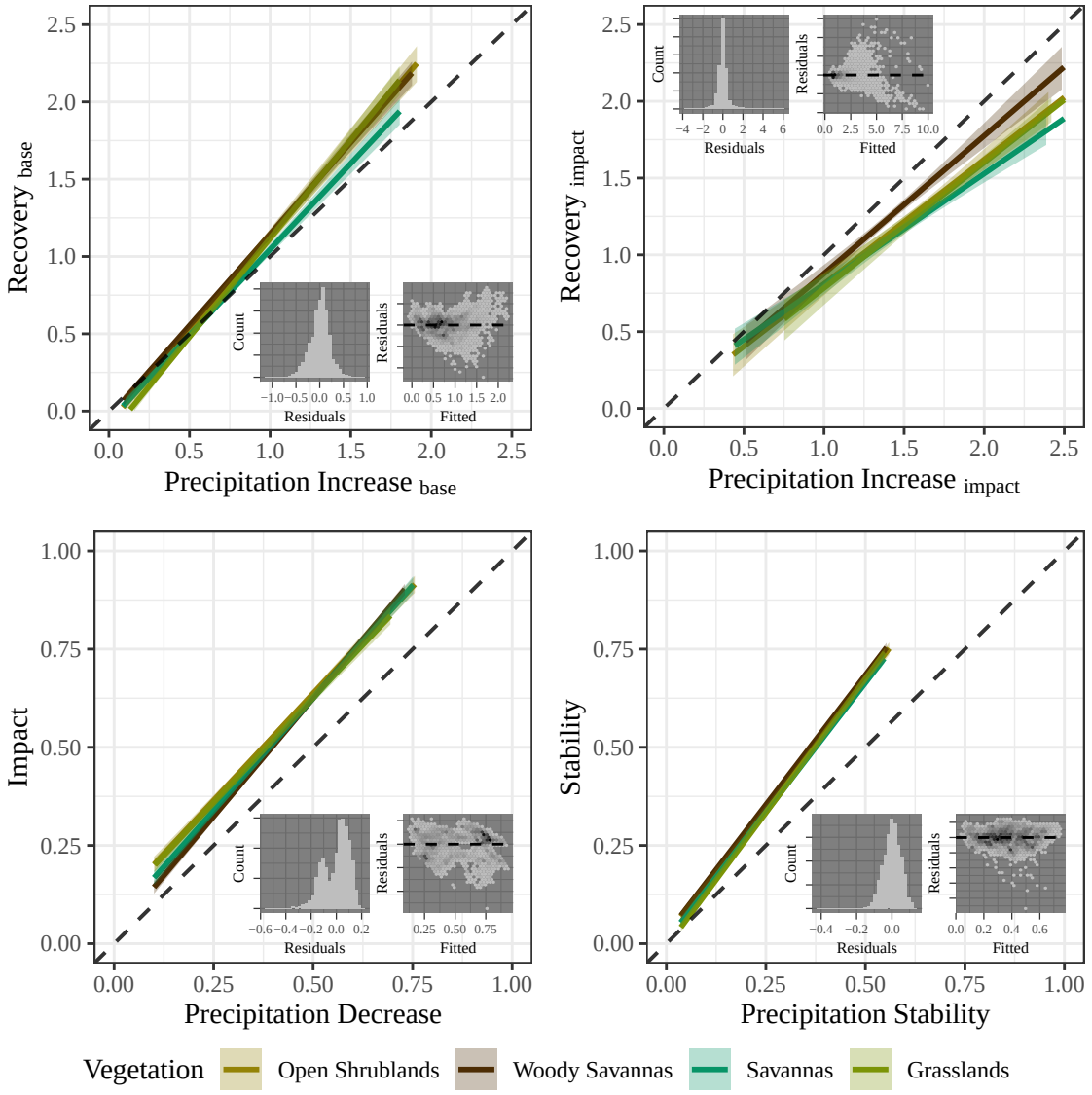

The shaded areas represent the 95% confidence interval for the regressions of each vegetation type, obtained by the sub-sampling process. Diagonal dashed line represent the 1:1 line. Dark gray plots are residuals, composed of the histogram of residuals and dispersion between residuals and fitted values, in which the horizontal dashed line is Residuals = 0.

SOURCE: Own production.

The coefficients of the regression between $Recovery_{base}$ and $Precipitation\ Increase_{base}$ show significant differences between the intercept of grasslands with the other vegetation types. The grasslands show a smaller intercept (positive difference between vegetation types minus Grasslands), while the slope shows differences between savannas and open shrublands, where the slope for savannas is lower in both cases. This indicates that savannas would present lower sensitivity to precipitation increases after a drought, and therefore less capacity to recover from this disturbance.

The differences found for $Recovery_{impact}$ and $Precipitation\ Increase_{impact}$ regressions were not significant with the exception of savannas against woody savannas, in which the first shows a reduced recovery capacity. More significant differences were found in the coefficients of the regressions between $Impact$ and $Precipitation\ Decrease$, where the intercept shows that woody savannas and savannas are more resistant (suffers less impact) than open shrublands and grasslands in the case of lower precipitation decreases, the slope shows significant differences between woody savannas against grasslands and open shrublands, being that the first one presents a higher slope than the others, which means that it is less resistant to drought as higher the precipitation decrease gets, in other words, the intercept and slope suggest that woody savannas are supposed to be more resistant to mild droughts, and less resistant to more intense droughts. The *Stability* regression shows differences in the intercept between woody savannas against savannas and grasslands, and open shrublands against grasslands. The woody savannas and open shrublands are less stable in cases when the variation of precipitation are smaller. The slope indicates that open shrublands are more stable (smaller slope) than grasslands in cases when the precipitation variations are higher.

The differences between the recovery components of the vegetation types can be represented in different ways. In this study we used one index normalized by the baseline, and one index normalized by the impact. From the results above it is possible to observe that the different recovery components showed different results. To explore the reasons for this behaviour we also analysed the relationship between the recovery components and the impact component.

Figure 4.10 - Differences between the intercept and slope of the linear regression between GPP and precipitation components of resilience.

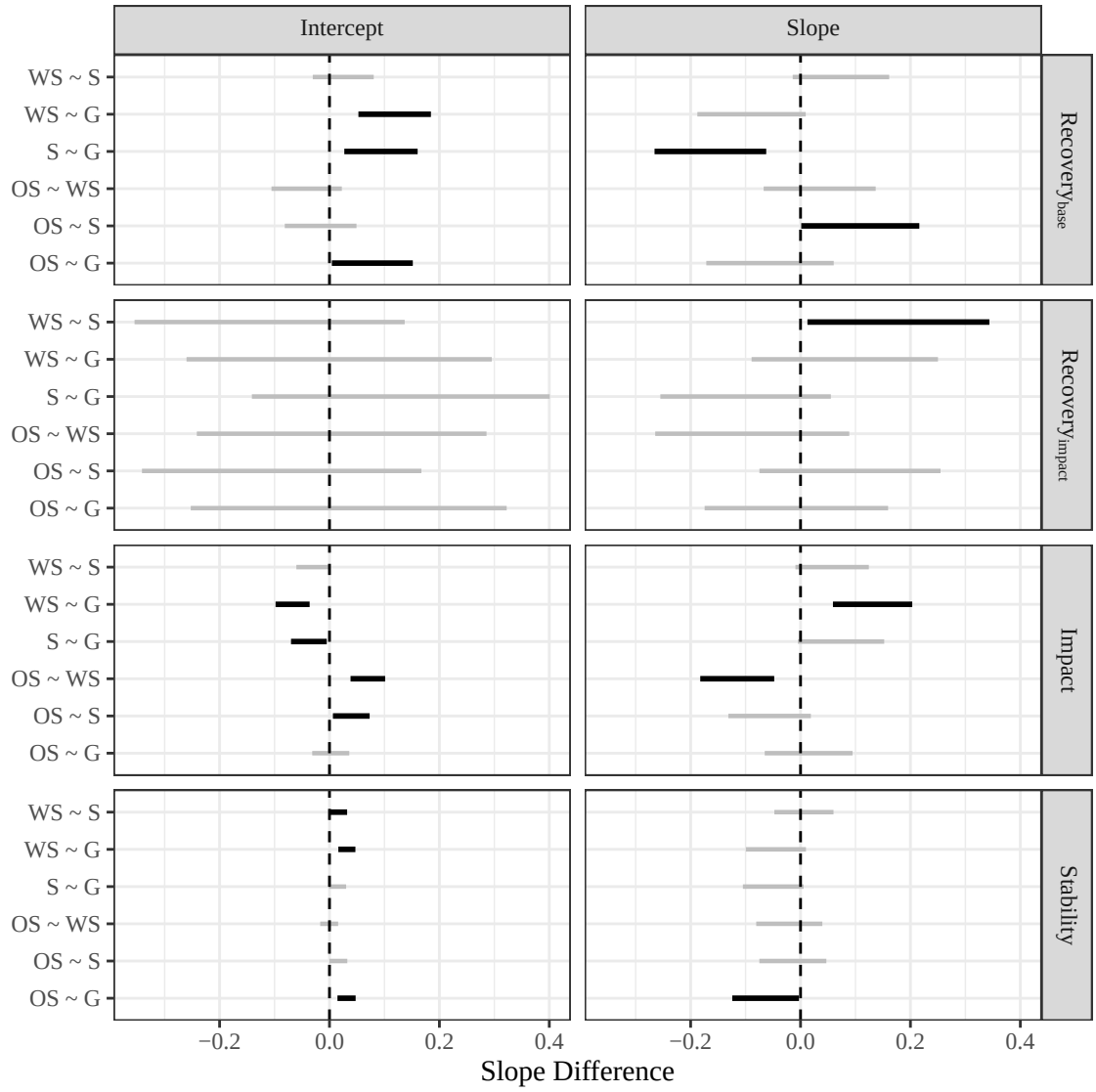

The horizontal solid lines represents the 95% confidence interval of the difference between the range of coefficients estimated by a sub-sampling procedure. Gray lines represents non significant differences, and black lines represents significant differences between vegetation types. The vertical dotted lines represents difference = 0, which indicates whether there is evidence or not to reject the hypothesis that the differences are not significant. The vegetation types are represented by abbreviations: Open Shrublands (OS), Woody Savannas (WS), Savannas (S), Grasslands (G).

SOURCE: Own production.

Figure 4.11 shows that the $Recovery_{base}$ has a positive correlation with $Impact$. This indicates that the larger the impact the larger the recovery. This is caused if there is a large reduction in GPP values, then there is also the possibility that the increase of this value to be even larger, by supposing that there is a limit of GPP for a certain vegetation type, and that there is no causation between $Impact$ and $Recovery_{base}$, what drives the recovery of the GPP is the annual precipitation, but this raise would be limited to the state of the system in the time where the recovery starts (which depends on the impact) and the GPP limit of this vegetation type. Thus, the recovery is heavily affected by the characteristics of the vegetation and the state of the system during the baseline and impact period.

Figure 4.11 - Dispersion between recovery and impact components.

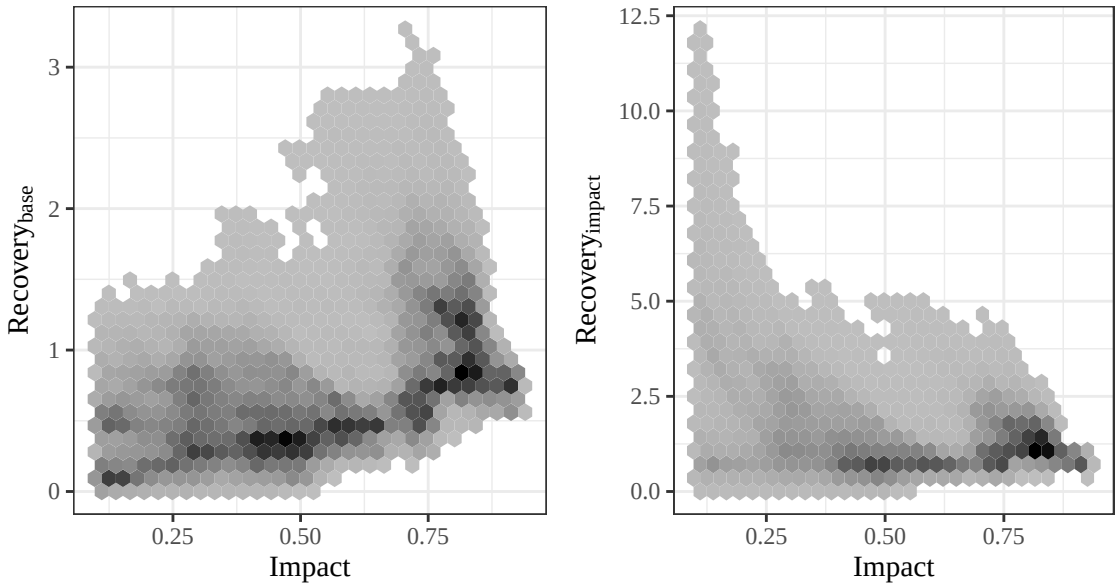

Gray hexagons represent areas with less concentration of paired values, black hexagons represents areas with a higher concentration of points.

SOURCE: Own production.

In the case of the relationship between $Recovery_{impact}$ and $Impact$, there is a negative correlation, in which the recovery has a large increase of values when the impact is lower than 0.25. This seems to be caused by the nature of the index, since we divide the absolute values of recovery by the absolute value of impact. Therefore, if the impact is small even if the recovery is relatively small in absolute terms, it can be

many times higher than the impact. This points to a high capacity of recovery in cases of reduced impacts, however, this creates an asymmetry in response to events based on the size of the impact.

By performing a series of linear regressions for each vegetation type, we can observe a significant difference between grasslands against the other vegetation types (Figure 4.12).

Figure 4.12 - Linear regressions between recovery and impact components of resilience for each vegetation type.

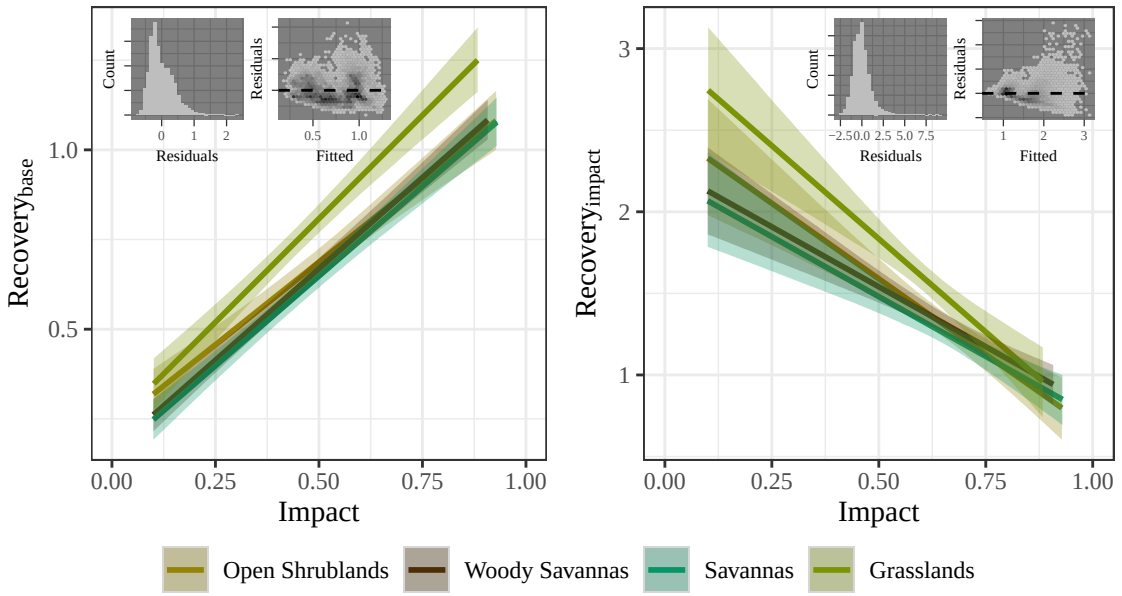

The shaded areas represents a 95% confidence interval for the regressions obtained by the sub-sampling process. Diagonal lines represent the 1:1 line. Dark gray plots are residuals, composed by histogram of residuals and dispersion between residuals and fitted values, in which the horizontal dashed line is Residuals = 0.

SOURCE: Own production.

The grasslands show higher recovery than other vegetation types, which implies that for the impact caused by precipitation decreases, the grasslands presented higher capacity to recover from the disturbance. In the case of $Recovery_{base}$, the higher recovery shown by grasslands could be explained by the intrinsic capacity of the vegetation to present a higher recovery even when the impact is higher, since there is no reason to believe that higher impact provides better condition for the veg-

etation to recover, specially since it presented to suffer higher $Impact$ than other vegetation types (Figure 4.10 and 4.7), so we can assume that even it has suffered more impact, this does not affect its capacity to recover. It could also be explained by the effect of another variable, such as the spatial variation of precipitation, or by both reasons acting together. In the case of $Recovery_{impact}$, the grasslands presents a higher recovery with smaller impact values than other vegetation types. However, it follows a steeper trajectory until it becomes equated with the other vegetation types for high impact values. This diverges from $Recovery_{base}$ and suggests that grasslands suffer more with larger impacts than the other vegetation types. This can also be explained by characteristics of the vegetation, or by spatial variation of precipitation.

4.4 Discussion

The study aimed to explore the differences between resilience components for different vegetation types. The results show that there are significant differences between the resilience components of different vegetation types. At least two vegetation types show significant differences in most of components and metrics examined here. Although it is worth reinforcing that we did not examine the potential impacts due to other variables, such as temperature or terrain characteristics.

As discussed by Stuart-Haëntjens et al. (2018), the resilience components are more influenced by annual precipitation variability than the characteristics of the ecosystem. This was also evidenced in Figure 4.6, where the distribution of the interquartile range of GPP components for each vegetation types followed closely the changes of the interquartile range of the precipitation components. The use of the factor between GPP and precipitation components was used to assess how each vegetation type was being affected by the variation of precipitation. This assumed that these differences could be related to intrinsic characteristics of the vegetation. Clearly it is imprecise to suppose that only the precipitation will have an impact in the GPP resilience components. However, it is known that in the Caatinga ecosystem considered here the interannual variation of temperature is small, and the vegetation productivity is primarily affected by the precipitation regime.

The practice of "normalizing" the system state indicator by the climatic variables should be adopted when analysing the resilience of vegetation to climatic anomalies. This was previously applied by Keersmaecker et al. (2015), who created a model relating NDVI anomalies and climatic anomalies (precipitation and temperature) at a global scale. They found differences in resistance and recovery (they referred to

these as resilience) in different regions of the planet. Their results showed that the Caatinga region has a medium to high capacity of recovery, a high sensitivity to drought impact, and a low susceptibility to temperature anomalies. Isbell et al. (2015) analysed the effect of biodiversity over resilience components by examining climatic variability to characterize the resilience components of vegetation of experimental areas by using a linear mixed-effects model.

It was observed that different recovery components show different results when comparing the median and regressions of the vegetation types, with even divergent results (Figure 4.9 and 4.12). It appears that the use of the $Recovery_{base}$ is more suitable to characterize the recovery of GPP after a drought event, since the interpretation of its results is in agreement with what was observed from the boxplots of the resilience components (Figure 4.6), and the *Stabilityresults* (Figure 4.9). There are numerous indices in the literature to estimate the resilience components in diverse applications Ingrisch and Bahn (2018), this can cause difficulties in achieving a comparability of studies approaching resilience. As suggested by Hodgson et al. (2015), we also recommend that simple and established metrics of impact (resistance) and recovery should be adopted, focusing on exploring the relationship between components calculated over different variables, instead of trying to develop an index that will robustly represent the resilience. Studies have reported a negative correlation between resistance (inverse of impact) and recovery (also named as resilience in some cases) (GAZOL et al., 2016; MACGILLIVRAY; GRIME, 1995; NIMMO et al., 2015; RUPPERT et al., 2014). In our results, we found contrary results, as in Figure 4.7, where woody savannas showed higher recovery and lower impact (higher resistance) than savannas. In addition, Figure 4.9 illustrates that grasslands show lower recovery under low precipitation increases, but higher recovery with high precipitation increases. This inversion also happens in the case of impact components in the same figure. The relationship between recovery and impact components are also sensitive to the index used to estimate them (Figure 4.12), as the correlation can change drastically, we believe that the concept that a vegetation which presents a higher resistance will necessarily have low recovery is risky and can be imprecise. The issue of many different indices to calculate recovery component was already explored by Ingrisch and Bahn (2018), Keersmaecker et al. (2014), however they should be analysed in more detail with different data sets in order to determine applicability across a wide range of conditions.

As the resilience is a complex concept, we realize that it would be more advantageous to characterize it in a qualitative manner, via interpretation of the estimations of

impact and recovery. To achieve a quantitative measurement of resilience would require an index able to represent its components symmetrically. However, as seen in this study, even the estimation of recovery is impacted by the impact, and it would be necessary to develop an index able to isolate the recovery from the impact. When adopting estimates of stability by using the coefficient of variation, we assume that its results translate the effect of both impact and recovery processes. However, this would not be symmetrical, for example, an ecosystem that presents a low impact and high recovery could have the same stability values as another ecosystem that suffered a large impact and presented low recovery. It would not be correct to assume that both of these systems are equally resilient. By analysing the stability components as a function between the system state indicator (in this case, GPP) and the disturbance driver (precipitation), we can analyse whether variations of the driver affect the indicator, and can therefore be useful to characterize a part of the resilience of the system, as a complement to the other components, and not by trying to quantify the resilience only using this one metric.

The study also illustrated that the relationship between GPP and precipitation variation is non-linear, which adds complexity to comparing the resilience of different ecosystems especially in a quantitative manner. By the results presented here, we show that the analysis of these relationships should be carried out in a series of steps. The study performed by Keersmaecker et al. (2015) showed the possibility of spatializing differences of resilience components globally. An alternative step could be taken by finding spatial clusters of regions with similar characteristics in resilience components in relation to climatic drivers. After separating these regions, a qualitative interpretation could be carried out in order to characterize these regions in a manner which would not necessarily rank them as being more or less resilient, but rather showing different aspects of resilience in different situations of disturbance and recovery.

The use of a LSM to estimate resilience components can present many problems, from the representation of the impact of precipitation over the vegetation productivity, to the oversimplified vegetation attributes and classes. However the use of process based models can present potential for this kind of study, since it can assess our current level of understanding relative to the underlying biophysical processes. This can have a significant impact on the estimates of resilience metrics ((KEERSMAECKER et al., 2015)). We recommend that additional studies comparing resilience components estimated by field data (eg. FLUXNET), LSMs and remote sensing derived data be carried out to access the current performance of LSMs to estimate

resilience of vegetation to drought.

4.5 Conclusions

The study performed a series of simulations conducted with the NOAH-MP LSM to represent the effect of drought in a semi-arid region. We analyzed the resilience of different vegetation types to the variation of precipitation caused by the drought and the posterior recovery. We found significant differences between vegetation types by relating GPP and precipitation variations through medians and linear regressions. Although relationships between the GPP and precipitation components were found to be non-linear, the linear regression were useful to show a range of aspects that can describe the resilience of vegetation. There is a possibility to expand the findings of previous studies by analysing this range of possibilities precipitation regimes to make more detailed assessment of resilience at a wide spatial extent.

5 CONCLUSIONS

Results from both chapters shows that:

a) NOAH-MP showed agreement with field measurements in an annual scales for carbon and energy fluxes. Although the impact of precipitation reduction was different between both sources, it is still viable to use NOAH-MP to simulate and explore the estimation of resilience of vegetation to droughts.

b) Simulation of different scenarios of drought and posterior recovery showed to be a useful tool to explore the estimation of resilience of vegetation to droughts. The results points that there are significant differences between the resilience of different vegetation types, even when they are distributed in an area with similar climate characteristics.

c) The estimation of resilience to droughts should be conducted by exploring the relationship between the affected subject of the system (vegetation) with the disturbance driver (precipitation), and that the analysis performed only with the relationship between impact and recovery should be done with caution.

d) The presented discussion points that the analysis of the resilience of a system to droughts should move towards the exploration of a range of climatic possibilities, that could be supplied with spatial and variability, and by the description of the relationship between the system subject and driver as a function (which showed to be non linear).

REFERENCES

AHLSTROM, A.; RAUPACH, M. R.; SCHURGERS, G.; SMITH, B.; ARNETH, A.; JUNG, M.; REICHSTEIN, M.; CANADELL, J. G.; FRIEDLINGSTEIN, P.; JAIN, A. K.; KATO, E.; POULTER, B.; SITCH, S.; STOCKER, B. D.; VIOVY, N.; WANG, Y. P.; WILTSHIRE, A.; ZAEHLE, S.; ZENG, N. The dominant role of semi-arid ecosystems in the trend and variability of the land CO2 sink. **Science**, v. 348, n. 6237, p. 895–899, may 2015. ISSN 0036-8075, 1095-9203. Available from: <http://www.sciencemag.org/cgi/doi/10.1126/science.aaa1668>. 9

ANDERSON, L. O.; RIBEIRO-NETO, G.; CUNHA, A. P.; FONSECA, M. G.; MOURA, Y. M. de; DALAGNOL, R.; WAGNER, F. H.; ARAGÃO, L. E. O. C. Vulnerability of amazonian forests to repeated droughts. **Philosophical Transactions of the Royal Society B: Biological Sciences**, v. 373, n. 1760, p. 20170411, oct. 2018. 9

BAI, Y.; WU, J.; XING, Q.; PAN, Q.; HUANG, J.; YANG, D.; HAN, X. Primary production and rain use efficiency across a precipitation gradient on the mongolia plateau. **Ecology**, v. 89, n. 8, p. 2140–2153, aug 2008. 8

BENTO, V. A.; GOUVEIA, C. M.; DACAMARA, C. C.; TRIGO, I. F. A climatological assessment of drought impact on vegetation health index. **Agricultural and Forest Meteorology**, v. 259, p. 286–295, sep 2018. 1

BEST, M. J.; ABRAMOWITZ, G.; JOHNSON, H. R.; PITMAN, A. J.; BALSAMO, G.; BOONE, A.; CUNTZ, M.; DECHARME, B.; DIRMEYER, P. A.; DONG, J.; EK, M.; GUO, Z.; HAVERD, V.; HURK, B. J. J. van den; NEARING, G. S.; PAK, B.; PETERS-LIDARD, C.; SANTANELLO, J. A.; STEVENS, L.; VUICHARD, N. The plumbing of land surface models: benchmarking model performance. **Journal of Hydrometeorology**, v. 16, n. 3, p. 1425–1442, jun. 2015. ISSN 1525-755X, 1525-7541. Available from: <http://journals.ametsoc.org/doi/10.1175/JHM-D-14-0158.1>. 10, 13, 15, 30

BRITO, S. S. B.; CUNHA, A. P. M. A.; CUNNINGHAM, C. C.; ALVALá, R. C.; MARENGO, J. A.; CARVALHO, M. A. Frequency, duration and severity of drought in the Semiarid Northeast Brazil region. **International Journal of Climatology**, v. 38, n. 2, p. 517–529, feb. 2018. ISSN 08998418. Available from: <http://doi.wiley.com/10.1002/joc.5225>. 9

COLLIER, N.; HOFFMAN, F. M.; LAWRENCE, D. M.; KEPPEL-ALEKS, G.; KOVEN, C. D.; RILEY, W. J.; MU, M.; RANDERSON, J. T. The international land model benchmarking (ILAMB) system: design, theory, and implementation. **Journal of Advances in Modeling Earth Systems**, v. 10, n. 11, p. 2731–2754, nov. 2018. 10

CUNHA, A. P. M. A.; ZERI, M.; LEAL, K. D.; COSTA, L.; CUARTAS, L. A.; MARENGO, J. A.; TOMASELLA, J.; VIEIRA, R. M.; BARBOSA, A. A.; CUNNINGHAM, C.; GARCIA, J. V. C.; BROEDEL, E.; ALVALÁ, R.; RIBEIRO-NETO, G. Extreme drought events over brazil from 2011 to 2019. **Atmosphere**, v. 10, n. 11, p. 642, oct. 2019. 9, 12

DAI, A.; ZHAO, T. Uncertainties in historical changes and future projections of drought. part i: estimates of historical drought changes. **Climatic Change**, v. 144, n. 3, p. 519–533, may 2016. 9

DAI, A.; ZHAO, T.; CHEN, J. Climate change and drought: a precipitation and evaporation perspective. **Current Climate Change Reports**, v. 4, n. 3, p. 301–312, may 2018. Available from: <https://doi.org/10.1007/s40641-018-0101-6>. 9

DRUMOND, M. A.; KIILL, L. H. P.; NASCIMENTO, C. E. S. Inventário e Sociabilidade de Espécies Arbóreas e Arbustivas da Caatinga na Região de Petrolina, PE. **Brasil Florestal**, v. 74, p. 37–43, 2002. 10

DU, L.; MIKLE, N.; ZOU, Z.; HUANG, Y.; SHI, Z.; JIANG, L.; MCCARTHY, H. R.; LIANG, J.; LUO, Y. Global patterns of extreme drought-induced loss in land primary production: identifying ecological extremes from rain-use efficiency. **Science of The Total Environment**, v. 628-629, p. 611–620, jul 2018. 1, 7

FRANK, D.; REICHSTEIN, M.; BAHN, M.; THONICKE, K.; FRANK, D.; MAHECHA, M. D.; SMITH, P.; VELDE, M. van der; VICCA, S.; BABST, F.; BEER, C.; BUCHMANN, N.; CANADELL, J. G.; CIAIS, P.; CRAMER, W.; IBROM, A.; MIGLIETTA, F.; POULTER, B.; RAMMIG, A.; SENEVIRATNE, S. I.; WALZ, A.; WATTENBACH, M.; ZAVALA, M. A.; ZSCHEISCHLER, J. Effects of climate extremes on the terrestrial carbon cycle: concepts, processes and potential future impacts. **Global Change Biology**, v. 21, n. 8, p. 2861–2880, may 2015. 1

FRIEDL, D. S.-M. M. **MCD12Q1 MODIS/Terra+Aqua Land Cover Type Yearly L3 Global 500m SIN Grid V006**. 2015. Available from: <https://lpdaac.usgs.gov/products/mcd12q1v006/>. 13, 37

GAZOL, A.; CAMARERO, J. J.; ANDEREGG, W. R. L.; VICENTE-SERRANO, S. M. Impacts of droughts on the growth resilience of northern hemisphere forests. **Global Ecology and Biogeography**, v. 26, n. 2, p. 166–176, sep 2016. 1, 7, 8, 41, 56

GUNDERSON, L. H. Ecological resilience—in theory and application. **Annual Review of Ecology and Systematics**, v. 31, n. 1, p. 425–439, nov 2000. 5

HODGSON, D.; MCDONALD, J. L.; HOSKEN, D. J. What do you mean, 'resilient'? **Trends in Ecology & Evolution**, v. 30, n. 9, p. 503–506, sep 2015. 5, 7, 33, 56

HOLLING, C. S. Resilience and stability of ecological systems. **Annual Review of Ecology and Systematics**, v. 4, n. 1, p. 1–23, nov 1973. 33

_____. Prologue: the scope of resilience engineering. In: SCHULZE, P. C. (Ed.). **Engineering Within Ecological Constraints**. Washington DC, USA: National Academy of Sciences Press, 1996. p. 31–43. 5

HOLLNAGEL, E. Prologue: the scope of resilience engineering. In: HOLLNAGEL, E.; PARIèS, J.; WOODS, D.; WREATHALL, J. (Ed.). **Resilience engineering in practice. A guidebook**. Farnham, Surrey, UK: Ashgate Publishing, 2010. p. 29–35. 5

HOOVER, D. L.; KNAPP, A. K.; SMITH, M. D. Resistance and resilience of a grassland ecosystem to climate extremes. **Ecology**, v. 95, n. 9, p. 2646–2656, sep 2014. 1, 5, 7, 8

HUANG, L.; HE, B.; CHEN, A.; WANG, H.; LIU, J.; LU, A.; CHEN, Z. Drought dominates the interannual variability in global terrestrial net primary production by controlling semi-arid ecosystems. **Scientific Reports**, v. 6, n. 1, apr. 2016. Available from: <http://www.nature.com/articles/srep24639>. 9

INGRISCH, J.; BAHN, M. Towards a comparable quantification of resilience. **Trends in Ecology & Evolution**, v. 33, n. 4, p. 251–259, apr 2018. 1, 2, 5, 6, 7, 33, 39, 41, 56

ISBELL, F.; CRAVEN, D.; CONNOLLY, J.; LOREAU, M.; SCHMID, B.; BEIERKUHNLEIN, C.; BEZEMER, T. M.; BONIN, C.; BRUELHEIDE, H.; LUCA, E. de; EBELING, A.; GRIFFIN, J. N.; GUO, Q.; HAUTIER, Y.; HECTOR, A.; JENTSCH, A.; KREYLING, J.; LANTA, V.; MANNING, P.; MEYER, S. T.; MORI, A. S.; NAEEM, S.; NIKLAUS, P. A.; POLLEY, H. W.; REICH, P. B.; ROSCHER, C.; SEABLOOM, E. W.; SMITH, M. D.; THAKUR, M. P.; TILMAN, D.; TRACY, B. F.; PUTTEN, W. H. van der; RUIJVEN, J. van; WEIGELT, A.; WEISSER, W. W.; WILSEY, B.; EISENHAUER, N. Biodiversity increases the resistance of ecosystem productivity to climate extremes. **Nature**, v. 526, n. 7574, p. 574–577, oct 2015. 7, 56

KAUWE, M. G. D.; ZHOU, S.-X.; MEDLYN, B. E.; PITMAN, A. J.; WANG, Y.-P.; DUURSMA, R. A.; PRENTICE, I. C. Do land surface models need to include differential plant species responses to drought? Examining model predictions across a mesic-xeric gradient in Europe. **Biogeosciences**, v. 12, n. 24, p. 7503–7518, dec. 2015. ISSN 1726-4189. Available from: <https://www.biogeosciences.net/12/7503/2015/>. 10, 30

KEENAN, T. F.; MIGLIAVACCA, M.; PAPALE, D.; BALDOCCHI, D.; REICHSTEIN, M.; TORN, M.; WUTZLER, T. Widespread inhibition of daytime ecosystem respiration. **Nature Ecology & Evolution**, v. 3, n. 3, p. 407–415, feb. 2019. Available from: <https://doi.org/10.1038/s41559-019-0809-2>. 13

KEERSMAECKER, W. D.; LHERMITTE, S.; HONNAY, O.; FARIFTEH, J.; SOMERS, B.; COPPIN, P. How to measure ecosystem stability? an evaluation of the reliability of stability metrics based on remote sensing time series across the major global ecosystems. **Global Change Biology**, v. 20, n. 7, p. 2149–2161, apr 2014. 33, 41, 56

KEERSMAECKER, W. D.; LHERMITTE, S.; TITS, L.; HONNAY, O.; SOMERS, B.; COPPIN, P. A model quantifying global vegetation resistance and resilience to short-term climate anomalies and their relationship with vegetation cover. **Global Ecology and Biogeography**, v. 24, n. 5, p. 539–548, feb 2015. 8, 55, 57

KNAPP, A. K. Variation among biomes in temporal dynamics of aboveground primary production. **Science**, v. 291, n. 5503, p. 481–484, jan 2001. 8

KNAPP, A. K.; CIAIS, P.; SMITH, M. D. Reconciling inconsistencies in precipitation-productivity relationships: implications for climate change. **New Phytologist**, v. 214, n. 1, p. 41–47, dec 2016. 1, 8

LAKE, P. S. Resistance, resilience and restoration. **Ecological Management & Restoration**, v. 14, n. 1, p. 20–24, dec 2012. 1, 5, 33

LEGATES, D. R.; MCCABE, G. J. Evaluating the use of "goodness-of-fit" measures in hydrologic and hydroclimatic model validation. **Water Resources Research**, v. 35, n. 1, p. 233–241, jan. 1999. ISSN 00431397. Available from: <http://doi.wiley.com/10.1029/1998WR900018>. 13, 14

_____. A refined index of model performance: a rejoinder. **International Journal of Climatology**, v. 33, n. 4, p. 1053–1056, mar. 2013. ISSN 08998418. Available from: <http://doi.wiley.com/10.1002/joc.3487>. 14, 26

LEWIS, S. L.; BRANDO, P. M.; PHILLIPS, O. L.; HEIJDEN, G. M. F. van der; NEPSTAD, D. The 2010 amazon drought. **Science**, v. 331, n. 6017, p. 554–554, feb. 2011. 9

LI, Z.; PENG, Y.; MA, X. Different response on drought tolerance and post-drought recovery between the small-leafed and the large-leafed white clover (trifolium repens l.) associated with antioxidative enzyme protection and lignin metabolism. **Acta Physiologiae Plantarum**, v. 35, n. 1, p. 213–222, aug 2012. 7

LLORET, F.; KEELING, E. G.; SALA, A. Components of tree resilience: effects of successive low-growth episodes in old ponderosa pine forests. **Oikos**, v. 120, n. 12, p. 1909–1920, jul 2011. 1, 5, 7, 8, 39

LUO, Y.; GERTEN, D.; MAIRE, G. L.; PARTON, W. J.; WENG, E.; ZHOU, X.; KEOUGH, C.; BEIER, C.; CIAIS, P.; CRAMER, W.; DUKES, J. S.; EMMETT, B.; HANSON, P. J.; KNAPP, A.; LINDER, S.; NEPSTAD, D.; RUSTAD, L. Modeled interactive effects of precipitation, temperature, and [CO2] on ecosystem carbon and water dynamics in different climatic zones. **Global Change Biology**, v. 14, n. 9, p. 1986–1999, sep 2008. 8

MACGILLIVRAY, C. W.; GRIME, J. P. Testing predictions of the resistance and resilience of vegetation subjected to extreme events. **Functional Ecology**, v. 9, n. 4, p. 640, aug 1995. 1, 5, 33, 56

MARENGO, J. A.; NOBRE, C. A.; TOMASELLA, J.; OYAMA, M. D.; OLIVEIRA, G. S. de; OLIVEIRA, R. de; CAMARGO, H.; ALVES, L. M.; BROWN, I. F. The drought of amazonia in 2005. **Journal of Climate**, v. 21, n. 3, p. 495–516, feb. 2008. 9

MARENGO, J. A.; TORRES, R. R.; ALVES, L. M. Drought in Northeast Brazil—past, present, and future. **Theoretical and Applied Climatology**, v. 129, n. 3-4, p. 1189–1200, aug. 2017. ISSN 0177-798X, 1434-4483. Available from: <http://link.springer.com/10.1007/s00704-016-1840-8>. 1, 9

NASH, J.; SUTCLIFFE, J. River flow forecasting through conceptual models part i — a discussion of principles. **Journal of Hydrology**, v. 10, n. 3, p. 282–290, apr. 1970. Available from: <https://doi.org/10.1016/0022-1694(70)90255-6>. 13, 14

NEARING, G. S.; RUDDELL, B. L.; CLARK, M. P.; NIJSSEN, B.; PETERS-LIDARD, C. Benchmarking and process diagnostics of land models. **Journal of Hydrometeorology**, v. 19, n. 11, p. 1835–1852, nov 2018. 10

NIMMO, D.; NALLY, R. M.; CUNNINGHAM, S.; HASLEM, A.; BENNETT, A. Vive la résistance: reviving resistance for 21st century conservation. **Trends in Ecology & Evolution**, v. 30, n. 9, p. 516–523, sep 2015. 7, 33, 56

NIU, G.-Y.; YANG, Z.-L.; MITCHELL, K. E.; CHEN, F.; EK, M. B.; BARLAGE, M.; KUMAR, A.; MANNING, K.; NIYOGI, D.; ROSERO, E.; TEWARI, M.; XIA, Y. The community Noah land surface model with multiparameterization options (Noah-MP): 1. Model description and evaluation with local-scale measurements. **Journal of Geophysical Research**, v. 116, n. D12, p. D12109, jun. 2011. ISSN 0148-0227. Available from: <http://doi.wiley.com/10.1029/2010JD015139>. 2, 12, 36, 37

ORLOWSKY, B.; SENEVIRATNE, S. I. Elusive drought: uncertainty in observed trends and short- and long-term CMIP5 projections. **Hydrology and Earth System Sciences**, v. 17, n. 5, p. 1765–1781, may 2013. 9

PENDERGRASS, A. G.; KNUTTI, R.; LEHNER, F.; DESER, C.; SANDERSON, B. M. Precipitation variability increases in a warmer climate. **Scientific Reports**, v. 7, n. 1, dec 2017. 1

POULTER, B.; FRANK, D.; CIAIS, P.; MYNENI, R. B.; ANDELA, N.; BI, J.; BROQUET, G.; CANADELL, J. G.; CHEVALLIER, F.; LIU, Y. Y.; RUNNING, S. W.; SITCH, S.; WERF, G. R. van der. Contribution of semi-arid ecosystems to interannual variability of the global carbon cycle. **Nature**, v. 509, n. 7502, p. 600–603, may 2014. ISSN 0028-0836, 1476-4687. Available from: <http://www.nature.com/articles/nature13376>. 9

PRENTICE, I. C.; LIANG, X.; MEDLYN, B. E.; WANG, Y.-P. Reliable, robust and realistic: the three r's of next-generation land-surface modelling. **Atmospheric Chemistry and Physics**, v. 15, n. 10, p. 5987–6005, may 2015. 9

PRETZSCH, H.; SCHüTZE, G.; UHL, E. Resistance of european tree species to drought stress in mixedversuspure forests: evidence of stress release by inter-specific facilitation. **Plant Biology**, v. 15, n. 3, p. 483–495, oct 2012. 1, 7

RATAJCZAK, Z.; CARPENTER, S. R.; IVES, A. R.; KUCHARIK, C. J.; RAMIADANTSOA, T.; STEGNER, M. A.; WILLIAMS, J. W.; ZHANG, J.; TURNER, M. G. Abrupt change in ecological systems: Inference and diagnosis. **Trends in Ecology & Evolution**, v. 33, n. 7, p. 513–526, jul 2018. 33

REZENDE, L. F. C.; ARENQUE-MUSA, B. C.; MOURA, M. S. B.; AIDAR, S. T.; RANDOW, C. V.; MENEZES, R. S. C.; OMETTO, J. P. B. H. Calibration of the maximum carboxylation velocity (vcmax) using data mining techniques and ecophysiological data from the brazilian semiarid region, for use in dynamic global vegetation models. **Brazilian Journal of Biology**, v. 76, n. 2, p. 341–351, mar. 2016. Available from: <https://doi.org/10.1590/1519-6984.14414>. 29

RODELL, M.; HOUSER, P. R.; JAMBOR, U.; GOTTSCHALCK, J.; MITCHELL, K.; MENG, C.-J.; ARSENAULT, K.; COSGROVE, B.; RADAKOVICH, J.; BOSILOVICH, M.; ENTIN, J. K.; WALKER, J. P.; LOHMANN, D.; TOLL, D. The global land data assimilation system. **Bulletin of the American Meteorological Society**, v. 85, n. 3, p. 381–394, mar. 2004. ISSN 0003-0007, 1520-0477. Available from: <http://journals.ametsoc.org/doi/10.1175/BAMS-85-3-381>. 12, 37

RUPPERT, J. C.; HARMONEY, K.; HENKIN, Z.; SNYMAN, H. A.; STERNBERG, M.; WILLMS, W.; LINSTäDTER, A. Quantifying drylands drought resistance and recovery: the importance of drought intensity, dominant life history and grazing regime. **Global Change Biology**, v. 21, n. 3, p. 1258–1270, nov 2014. 56

SCHAEFLI, B.; GUPTA, H. V. Do Nash values have value? **Hydrological Processes**, v. 21, n. 15, p. 2075–2080, jul. 2007. ISSN 08856087, 10991085. Available from: <http://doi.wiley.com/10.1002/hyp.6825>. 14

SCHEFFER, M.; CARPENTER, S. R.; DAKOS, V.; NES, E. H. van. Generic indicators of ecological resilience: inferring the chance of a critical transition.

Annual Review of Ecology, Evolution, and Systematics, v. 46, n. 1, p. 145–167, dec 2015. 41

SHERWOOD, S.; FU, Q. A drier future? **Science**, v. 343, n. 6172, p. 737–739, feb. 2014. 9

SIPPEL, S.; REICHSTEIN, M.; MA, X.; MAHECHA, M. D.; LANGE, H.; FLACH, M.; FRANK, D. Drought, heat, and the carbon cycle: a review. **Current Climate Change Reports**, v. 4, n. 3, p. 266–286, jun 2018. 1, 8

SOUZA, L. S. B. d.; MOURA, M. S. B. de; SEDIYAMA, G. C.; SILVA, T. G. F. da. Carbon exchange in a caatinga area during an unusually drought year. **Agrometeoros**, v. 25, n. 1, 2018. 10, 13

SPINONI, J.; NAUMANN, G.; VOGT, J. V.; BARBOSA, P. The biggest drought events in Europe from 1950 to 2012. **Journal of Hydrology: Regional Studies**, v. 3, p. 509–524, mar. 2015. 9

STUART-HAëNTJENS, E.; BOECK, H. J. D.; LEMOINE, N. P.; MäND, P.; KRöEL-DULAY, G.; SCHMIDT, I. K.; JENTSCH, A.; STAMPFLI, A.; ANDEREGG, W. R.; BAHN, M.; KREYLING, J.; WOHLGEMUTH, T.; LLORET, F.; CLASSEN, A. T.; GOUGH, C. M.; SMITH, M. D. Mean annual precipitation predicts primary production resistance and resilience to extreme drought. **Science of The Total Environment**, v. 636, p. 360–366, sep 2018. 1, 2, 7, 8, 55

TODMAN, L. C.; FRASER, F. C.; CORSTANJE, R.; DEEKS, L. K.; HARRIS, J. A.; PAWLETT, M.; RITZ, K.; WHITMORE, A. P. Defining and quantifying the resilience of responses to disturbance: a conceptual and modelling approach from soil science. **Scientific Reports**, v. 6, n. 1, jun 2016. 6

TRENBERTH, K. E.; DAI, A.; SCHRIER, G. van der; JONES, P. D.; BARICHIVICH, J.; BRIFFA, K. R.; SHEFFIELD, J. Global warming and changes in drought. **Nature Climate Change**, v. 4, n. 1, p. 17–22, dec. 2013. 9

WALKER, B.; HOLLING, C. S.; CARPENTER, S. R.; KINZIG, A. P. Resilience, adaptability and transformability in social-ecological systems. **Ecology and Society**, v. 9, n. 2, 2004. 33

WILCOX, K. R.; BLAIR, J. M.; SMITH, M. D.; KNAPP, A. K. Does ecosystem sensitivity to precipitation at the site-level conform to regional-scale predictions? **Ecology**, dec 2015. 8

WILLMOTT, C. J.; ROBESON, S. M.; MATSUURA, K.; FICKLIN, D. L. Assessment of three dimensionless measures of model performance. **Environmental Modelling & Software**, v. 73, p. 167–174, nov. 2015. ISSN 13648152. Available from: <https://linkinghub.elsevier.com/retrieve/pii/S1364815215300384>. 14

WU, D.; CIAIS, P.; VIOVY, N.; KNAPP, A. K.; WILCOX, K.; BAHN, M.; SMITH, M. D.; VICCA, S.; FATICHI, S.; ZSCHEISCHLER, J.; HE, Y.; LI, X.; ITO, A.; ARNETH, A.; HARPER, A.; UKKOLA, A.; PASCHALIS, A.; POULTER, B.; PENG, C.; RICCIUTO, D.; REINTHALER, D.; CHEN, G.; TIAN, H.; GENET, H.; MAO, J.; INGRISCH, J.; NABEL, J. E. S. M.; PONGRATZ, J.; BOYSEN, L. R.; KAUTZ, M.; SCHMITT, M.; MEIR, P.; ZHU, Q.; HASIBEDER, R.; SIPPEL, S.; DANGAL, S. R. S.; SITCH, S.; SHI, X.; WANG, Y.; LUO, Y.; LIU, Y.; PIAO, S. Asymmetric responses of primary productivity to altered precipitation simulated by ecosystem models across three long-term grassland sites. **Biogeosciences**, v. 15, n. 11, p. 3421–3437, jun 2018. 8

WU, Z.; DIJKSTRA, P.; KOCH, G. W.; PEÑUELAS, J.; HUNGATE, B. A. Responses of terrestrial ecosystems to temperature and precipitation change: a meta-analysis of experimental manipulation. **Global Change Biology**, v. 17, n. 2, p. 927–942, jan 2011. 8

YANG, Y.; FANG, J.; MA, W.; WANG, W. Relationship between variability in aboveground net primary production and precipitation in global grasslands. **Geophysical Research Letters**, v. 35, n. 23, dec 2008. 8

ZANG, C.; HARTL-MEIER, C.; DITTMAR, C.; ROTHE, A.; MENZEL, A. Patterns of drought tolerance in major european temperate forest trees: climatic drivers and levels of variability. **Global Change Biology**, v. 20, n. 12, p. 3767–3779, jun 2014. 41

ZHANG, B.; DENG, H.; WANG, H. li; YIN, R.; HALLETT, P. D.; GRIFFITHS, B. S.; DANIELL, T. J. Does microbial habitat or community structure drive the functional stability of microbes to stresses following re-vegetation of a severely degraded soil? **Soil Biology and Biochemistry**, v. 42, n. 5, p. 850–859, may 2010. 5

ZHAO, T.; DAI, A. Uncertainties in historical changes and future projections of drought. part II: model-simulated historical and future drought changes. **Climatic Change**, v. 144, n. 3, p. 535–548, jul. 2016. 9

ZHOU, S.-X.; PRENTICE, I. C.; MEDLYN, B. E. Bridging drought experiment and modeling: Representing the differential sensitivities of leaf gas exchange to drought. **Frontiers in Plant Science**, v. 9, jan. 2019. Available from: <https://doi.org/10.3389/fpls.2018.01965>. 29

ZSCHEISCHLER, J.; MICHALAK, A. M.; SCHWALM, C.; MAHECHA, M. D.; HUNTZINGER, D. N.; REICHSTEIN, M.; BERTHIER, G.; CIAIS, P.; COOK, R. B.; EL-MASRI, B.; HUANG, M.; ITO, A.; JAIN, A.; KING, A.; LEI, H.; LU, C.; MAO, J.; PENG, S.; POULTER, B.; RICCIUTO, D.; SHI, X.; TAO, B.; TIAN, H.; VIOVY, N.; WANG, W.; WEI, Y.; YANG, J.; ZENG, N. Impact of large-scale climate extremes on biospheric carbon fluxes: an intercomparison based on MsTMIP data. **Global Biogeochemical Cycles**, v. 28, n. 6, p. 585–600, jun 2014. 8

ZSCHEISCHLER, J.; REICHSTEIN, M.; HARMELING, S.; RAMMIG, A.; TOMELLERI, E.; MAHECHA, M. D. Extreme events in gross primary production: a characterization across continents. **Biogeosciences**, v. 11, n. 11, p. 2909–2924, jun 2014. 1

PUBLICAÇÕES TÉCNICO-CIENTÍFICAS EDITADAS PELO INPE

Teses e Dissertações (TDI)

Teses e Dissertações apresentadas nos Cursos de Pós-Graduação do INPE.

Notas Técnico-Científicas (NTC)

Incluem resultados preliminares de pesquisa, descrição de equipamentos, descrição e ou documentação de programas de computador, descrição de sistemas e experimentos, apresentação de testes, dados, atlas, e documentação de projetos de engenharia.

Propostas e Relatórios de Projetos (PRP)

São propostas de projetos técnico-científicos e relatórios de acompanhamento de projetos, atividades e convênios.

Publicações Seriadas

São os seriados técnico-científicos: boletins, periódicos, anuários e anais de eventos (simpósios e congressos). Constam destas publicações o Internacional Standard Serial Number (ISSN), que é um código único e definitivo para identificação de títulos de seriados.

Pré-publicações (PRE)

Todos os artigos publicados em periódicos, anais e como capítulos de livros.

Manuais Técnicos (MAN)

São publicações de caráter técnico que incluem normas, procedimentos, instruções e orientações.

Relatórios de Pesquisa (RPQ)

Reportam resultados ou progressos de pesquisas tanto de natureza técnica quanto científica, cujo nível seja compatível com o de uma publicação em periódico nacional ou internacional.

Publicações Didáticas (PUD)

Incluem apostilas, notas de aula e manuais didáticos.

Programas de Computador (PDC)

São a seqüência de instruções ou códigos, expressos em uma linguagem de programação compilada ou interpretada, a ser executada por um computador para alcançar um determinado objetivo. Aceitam-se tanto programas fonte quanto os executáveis.